

cy.7

OKB

AUG 1 1973  
APR 22 1975

SECRET



# VISCOUS EFFECTS IN LOW-DENSITY NOZZLE FLOWS

David L. Whitfield

ARO, Inc.

June 1973

Approved for public release; distribution unlimited.

**VON KÁRMÁN GAS DYNAMICS FACILITY  
ARNOLD ENGINEERING DEVELOPMENT CENTER  
AIR FORCE SYSTEMS COMMAND  
ARNOLD AIR FORCE STATION, TENNESSEE**

Property of U. S. Air Force  
AEDC LIBRARY  
EX-100-1-1-1

# ***NOTICES***

When U. S. Government drawings, specifications, or other data are used for any purpose other than a definitely related Government procurement operation, the Government thereby incurs no responsibility nor any obligation whatsoever, and the fact that the Government may have formulated, furnished, or in any way supplied the said drawings, specifications, or other data, is not to be regarded by implication or otherwise, or in any manner licensing the holder or any other person or corporation, or conveying any rights or permission to manufacture, use, or sell any patented invention that may in any way be related thereto.

Qualified users may obtain copies of this report from the Defense Documentation Center.

References to named commercial products in this report are not to be considered in any sense as an endorsement of the product by the United States Air Force or the Government.

# VISCOUS EFFECTS IN LOW-DENSITY NOZZLE FLOWS

David L. Whitfield  
ARO, Inc.

Approved for public release; distribution unlimited.

## FOREWORD

The work reported herein was conducted by the Arnold Engineering Development Center (AEDC) under the sponsorship of the Air Force Rocket Propulsion Laboratory (AFRPL), Air Force Systems Command (AFSC), under Program Element 62302F. This work was monitored by Captain Sam Thompson of AFRPL.

The results presented were obtained by ARO, Inc. (a subsidiary of Sverdrup & Parcel and Associates, Inc.), contract operator of the Arnold Engineering Development Center (AEDC), AFSC, Arnold Air Force Station, Tennessee. The work was conducted from March 9 to November 30, 1972, under ARO Project Nos. VY0202 and VC097. The manuscript was submitted for publication on January 18, 1973.

This technical report has been reviewed and is approved.

JIMMY W. MULLINS  
Lt Colonel, USAF  
Chief Air Force Test Director, VKF  
Directorate of Test

A. L. COAPMAN  
Colonel, USAF  
Director of Test

## ABSTRACT

Viscous effects in low-density nozzle flows were investigated numerically, and comparisons were made with experimental data. The numerical method of Patankar and Spalding was modified to solve the internal laminar boundary-layer equations for two-dimensional flow or axisymmetric flow with or without transverse curvature. A listing is given of the computer code. Boundary-layer displacement thicknesses for typical nozzle geometries and flow conditions are presented. Solutions were obtained for specific conditions corresponding to experimental data. The result is a relatively fast, simple to use numerical procedure, which is shown to give results in good agreement with experimental data.

## CONTENTS

	<u>Page</u>
ABSTRACT . . . . .	iii
NOMENCLATURE . . . . .	vii
I. INTRODUCTION . . . . .	1
II. BASIC EQUATIONS	
2.1 Governing Equations . . . . .	3
2.2 Nondimensionalized Equations . . . . .	5
2.3 Transformed Equations . . . . .	7
III. NUMERICAL SOLUTION	
3.1 Basic Scheme . . . . .	9
3.2 Input Conditions . . . . .	11
3.3 Some Possible Computational Difficulties . . . . .	14
IV. NUMERICAL RESULTS . . . . .	16
V. COMPARISONS WITH EXPERIMENTAL DATA AND OTHER THEORETICAL RESULTS . . . . .	18
VI. CONCLUSIONS . . . . .	21
REFERENCES . . . . .	22

## APPENDIXES

### I. ILLUSTRATIONS

#### Figure

1. Definition of Coordinate System . . . . .	27
2. Displacement Thickness of Successive Iterations for Condition No. 5 (Table I) . . . . .	28
3. Displacement Thickness for Condition No. 1 (Table I) . . . . .	29
4. Displacement Thickness for Condition No. 2 (Table I) . . . . .	30
5. Displacement Thickness for Condition No. 3 (Table I) . . . . .	31
6. Displacement Thickness for Condition No. 4 (Table I) . . . . .	32

<u>Figure</u>	<u>Page</u>
7. Displacement Thickness for Condition No. 5 (Table I) . . . . .	33
8. Displacement Thickness for Condition No. 6 (Table I) . . . . .	34
9. Displacement Thickness for Condition No. 7 (Table I) . . . . .	35
10. Displacement Thickness for Condition No. 8 (Table I) . . . . .	36
11. Nozzle Exit Velocity and Temperature Profiles for Condition Nos. 3 and 9 (Table I) . . . . .	37
12. Displacement Thicknesses of an Axisymmetric and Two-Dimensional Nozzle with Equal Area Ratios . . . . .	38
13. Reservoir Reynolds Number as a Function of $p_o$ , $T_o$ , and $r^*$ for Various Gases . . . . .	39
14. Calculated and Measured Pitot Pressure Profiles at the M3 Nozzle Throat for $Re_{o,r^*} = 900$ . . . . .	40
15. Calculated and Measured Pitot Pressure Profiles at the M3 Nozzle Exit for $Re_{o,r^*} = 1800$ . . . . .	41
16. Calculated and Measured Pitot Pressure Profiles at the Nozzle Exit for $Re_{o,r^*} = 900$ . . . . .	42
17. Calculated and Measured Pitot Pressure Profiles at the M3 Nozzle Exit for $Re_{o,r^*} = 4500$ . . . . .	43
18. Calculated and Measured Pitot Pressure Profiles Down- stream of the M3 Nozzle Throat for $Re_{o,r^*} = 1170$ . . . . .	44
19. Calculated and Measured Pitot Pressure Profiles Down- stream of the M3 Nozzle Throat for $Re_{o,r^*} = 330$ . . . . .	45
20. Calculated Velocity, Temperature, and Pitot Pressure Profiles Downstream of the M3 Nozzle Throat for $Re_{o,r^*} = 330$ . . . . .	46
21. Calculated and Measured Heat-Transfer Coefficients in a Low-Density Nozzle . . . . .	47

	<u>Page</u>
II. TABLE	
I. Conditions for the Numerical Solutions Presented in Section IV . . . . .	48
III. BOUNDARY-LAYER COMPUTER CODE . . . . .	49
IV. INITIAL PRESSURE DISTRIBUTION COMPUTER CODE . . . . .	67

## NOMENCLATURE

$A$	Cross-sectional area of nozzle
$c_p$	Specific heat at constant pressure
$c_v$	Specific heat at constant volume
$d^*$	Nozzle throat diameter
$H$	Local total enthalpy
$\bar{H}$	$H/H_0$
$h$	Heat-transfer coefficient
$k$	Thermal conductivity
$M$	Mach number
$\dot{m}$	Mass flux
$Pr$	Prandtl number, $\mu c_p/k$
$p$	Pressure
$p_p$	Measured pitot pressure
$\bar{p}$	$(\gamma - 1)p/(\gamma p_0)$
$q_w$	Nozzle wall heat-transfer rate
$R$	Longitudinal radius of curvature of converging portion of nozzle
$\bar{R}$	$R/r^*$
$Re_{0,r^*}$	Nozzle reservoir Reynolds number, $\rho_0(2H_0)^{1/2}r^*/\mu_0$



$r$	Defined by Eq. (4)
$\bar{r}$	$r/r^*$
$r^*$	Nozzle throat radius
$T$	Temperature
$T_{aw}$	Adiabatic wall temperature
$\bar{T}$	$T/T_O$
$u$	Velocity component in x direction
$\bar{u}$	$u/(H_O)^{1/2}$
$v$	Velocity component in y direction
$\bar{v}$	$v/(H_O)^{1/2}$
$x$	Coordinate along nozzle wall
$\bar{x}$	$x/r^*$
$y$	Coordinate normal to nozzle wall
$\bar{y}$	$y/r^*$
$z$	Coordinate along nozzle axis referenced to the throat
$\bar{z}$	$z/r^*$
$\alpha$	Nozzle wall angle
$\gamma$	$c_p/c_v$
$\delta$	Boundary-layer thickness defined as the value of $y$ where $u/u_E = 0.99$
$\delta^*$	Boundary-layer displacement thickness
$\xi$	Exponent in power law viscosity, $\mu \sim T^\xi$
$\eta$	$\bar{y}/\bar{y}_E$
$\mu$	Viscosity
$\bar{\mu}$	$\mu/\mu_O$
$\nu$	Denotes planar or axisymmetric flow in Eq. (23)
$\xi$	Transformed x coordinate, Eq. (11)
$\rho$	Mass density
$\bar{\rho}$	$\rho/\rho_O$

$\psi$	Stream function
$\omega$	Transformed stream function, Eq. (12)

**SUPERSCRIPT**

Condition immediately downstream of a normal shock

**SUBSCRIPTS**

$\zeta_L$	Nozzle centerline
E	Outer edge of boundary layer
e	Nozzle exit
I	Inner edge of boundary layer
o	Reservoir (total) conditions
w	Nozzle wall

## SECTION I INTRODUCTION

Investigations of viscous effects in low-density gas flows in two-dimensional and axisymmetric channels and nozzles have been conducted during the past few years in support of the design of low-density wind tunnel facilities and small microthrust rockets used for spacecraft attitude control. In addition to these areas of interest, there are two other areas where attention to viscous effects is required. One is that of internal boundary-layer scaling. When the nozzle and/or plume flow of a rocket engine is to be investigated in a wind tunnel or space chamber, it is usually necessary to significantly reduce the size of the nozzle used. To achieve adequate simulation, the model nozzle viscous effects must appropriately simulate those of the actual rocket. A specific example of this problem is found in the laboratory study of rocket exhaust plumes interacting with the free-stream (Ref. 1). The other area of interest is associated with the study of gas dynamic and chemical lasers (Ref. 2). The total laser power output is influenced by the static gas pressure in the optical cavity just downstream of the nozzle exit. Since the nozzles used are small and since they operate at relatively high total temperatures, the nozzle viscous effects significantly influence the nozzle static pressure distribution. Although numerous comparisons with experimental data from low-density wind tunnel nozzles will be presented to check the accuracy of the results, the present investigation was motivated by the current interest in rocket nozzle scaling and the viscous effects on the operation of gas dynamic and chemical laser systems.

Some previous investigations of the design and analysis of low-density wind tunnel nozzles are given in Refs. 3 through 5. The method of Potter and Carden (Ref. 3) was developed to design nozzles for particular test section flow conditions. It is based on an integral technique which uses the similar solutions of Cohen and Reshotko (Ref. 6). Although the work of Potter and Carden (Ref. 3) has proved successful for the design of nozzles to produce desired flow conditions, it is not directly applicable to the analysis of specified nozzle geometry. Also, non-similar solutions presented in Ref. 4 indicate that similarity does not exist in nozzle flows, particularly near the throat, and as a consequence, inaccuracies may result from the use of similar solutions for relatively short nozzles.

The method presented in Refs. 4 and 5 solves the non-similar laminar boundary-layer equations with or without first-order transverse curvature (referred to as second-order in Refs. 4 and 7), with or without velocity slip and temperature jump boundary conditions, and it has been shown to be accurate. However, the method has certain disadvantages: (1) the numerical integration scheme is that of Jaffe, Lind, and Smith (Ref. 7) which requires a relatively large amount of computer time, (2) the computer program is large and not necessarily simple to use, (3) the transformation variables are not amenable to internal flow problems, and (4) large flow expansions frequently require interpolating the solutions, changing the numerical step size across the nozzle, and resuming the calculations. These disadvantages discourage the use of the method described in Refs. 4 and 5.

The methods described in Refs. 3 through 5 assume that the nozzle flow consists of a viscous region and an inviscid (core) region. Some previous investigations which are not restricted to such flows, but permit viscous effects across the entire channel, are described in Refs. 8 through 10. These investigations are more suitable for the study of flow in microthrust rockets where the flow may be fully viscous. However, these methods also have certain disadvantages for the present application. The works of Adams (Ref. 8) and Williams (Ref. 9) are based on similar solutions, the conditions for which are not likely to be satisfied by a large class of practical problems. The work of Rae (Ref. 10) is a significant contribution to the study of low-density nozzle flows, and this method will be discussed further in this report. Numerical results from Rae's method will be compared with results from Ref. 5, results obtained in the present investigation, and experimental data. Rae's method was shown to give good results for fully viscous flows (Ref. 10); however, it will be shown herein to be less accurate than the method of Refs. 4 and 5 or the present method for the flow regime of interest in this investigation.

The objectives of the present investigation are: (1) to provide results for estimating the viscous effects in low-density converging-diverging nozzle flows based on certain flow parameters and nozzle geometries, and (2) to provide a fast, simple to use method for calculating viscous effects in low-density nozzle flows. To meet these objectives, the numerical integration scheme of Patankar and Spalding (Ref. 11) was used. In fact, the program used for this work was taken directly from Ref. 11 and then suitably modified for internal, low-density flows. The resulting program is similar to that of Mayne (Ref. 2) except for the numerical scheme used near the wall. Also, the

present work is based on a set of dimensionless equations which reduces the amount of input and provides more convenient solutions in the sense that they are applicable to flows which satisfy certain parameters rather than specific inputs of pressure, temperature, etc.

The following section describes the governing equations and boundary conditions, the variables used to nondimensionlize the equations, and the transformed equations. Section III describes briefly the numerical solution as well as some of the computational difficulties which have been encountered with this program. Section IV is devoted to numerical results and Section V to comparisons of the present results with previous theoretical investigations and experimental data. Some conclusions are given in Section VI.

## SECTION II BASIC EQUATIONS

The governing system of equations and the boundary conditions are presented in this section. Certain dimensionless and transformation variables are introduced and used to transform the governing equations for convenience of the numerical solution. Also, the boundary-layer displacement thickness is derived in the transformed plane. Although the program will solve the two-dimensional equations or axisymmetric equations with or without transverse curvature, only the equations appropriate to the latter with the transverse curvature terms retained are considered here in detail because they are more general. The two-dimensional equations can be obtained from the equations considered by setting  $r \equiv 1$ , and the axisymmetric equations without transverse curvature can be obtained by setting  $r \equiv r_w$ .

### 2.1 GOVERNING EQUATIONS

The governing system of equations is taken as that obtained by Probstein and Elliott (Ref. 12). The equations in curvilinear coordinates are:

#### Continuity Equation

$$\frac{\partial(\rho ur)}{\partial x} + \frac{\partial(\rho vr)}{\partial y} = 0 \quad (1)$$

## Momentum Equation

$$\rho u \frac{\partial u}{\partial x} + \rho v \frac{\partial u}{\partial y} = -\frac{dp}{dx} + \frac{1}{r} \frac{\partial}{\partial y} \left( r \mu \frac{\partial u}{\partial y} \right) \quad (2)$$

## Total Energy Equation

$$\rho u \frac{\partial H}{\partial x} + \rho v \frac{\partial H}{\partial y} = \frac{1}{r} \frac{\partial}{\partial y} \left\{ r \left[ \frac{\mu}{Pr} \frac{\partial H}{\partial y} + \mu \left( 1 - \frac{1}{Pr} \right) u \frac{\partial u}{\partial y} \right] \right\} \quad (3)$$

The total energy equation is obtained by multiplying the momentum equation by  $u$  and adding the result to the static energy equation. The coordinate system is defined in Fig. 1 (Appendix I) with the  $r(x, y)$  term defined for internal flow as

$$r(x, y) = r_w(x) - y \cos \alpha \quad (4)$$

Probstein and Elliott (Ref. 12) obtained Eqs. (1) through (3) by an order of magnitude analysis of the general forms of the continuity equation, Navier-Stokes momentum equations, and energy equation. The assumptions made in the analysis were that the ratio of the boundary-layer thickness to the longitudinal radius of curvature of the body surface was small compared to unity, and the ratio of the boundary-layer thickness to the nozzle radius was on the order of unity. Therefore, Eqs. (1) through (3) are valid for nozzles which have a longitudinal radius of curvature much larger than the nozzle radius. This stipulation is normally satisfied by axisymmetric convergent-divergent nozzles used for low-density wind tunnels, rockets, and gas dynamic and chemical laser systems.

The axisymmetric boundary-layer equations without transverse curvature terms correspond to those which can be obtained from Eqs. (1) through (3) by replacing  $r(x, y)$  with  $r_w(x)$  as stated above. Because  $r_w(x)$  is a function of  $x$  only, it can be eliminated from Eqs. (2) and (3), and therefore appears only in the continuity equation. The resulting set of equations can be used to describe internal or external boundary layers. It was shown in Ref. 5, by solutions with and without the transverse curvature terms, that the effect of transverse curvature is important for  $\delta/r_w(x) \sim 0(1)$ .

Implicit in Eq. (2) by the use of the total derivative of  $p$  with respect to  $x$  is the  $y$  component of the momentum equation as given by

$$-\frac{\partial p}{\partial y} = 0 \quad (5)$$

The validity of this equation is sometimes questioned for thick laminar boundary layers. However, the analysis of Probst and Elliott (Ref. 12) indicates that this equation is consistent with the other equations in the governing set. Equation (5) was used in Refs. 4 and 5, and good agreement between calculated and measured boundary-layer profiles was obtained for flow conditions where 99 percent of the cross-sectional area of a nozzle was boundary layer.

For the boundary conditions at the edge of the boundary layer, it was assumed that an isentropic core flow exists along the nozzle centerline, from which the flow properties at the edge of the boundary layer can be calculated. The boundary conditions at the nozzle wall were taken as zero velocity and a prescribed wall temperature distribution or a prescribed wall heat-transfer distribution. Solutions were presented in Ref. 5 with and without velocity slip and temperature jump boundary conditions. For the conditions investigated in Ref. 5, it was found that the nozzle flow merged (that is, the boundary layer completely filled the nozzle) before velocity slip and temperature jump became significant. Therefore, no-slip wall boundary conditions were assumed adequate for this investigation.

The system of equations is completed by using the equation of state,  $p = \rho RT$ , and expressing the viscosity as some function of  $T$ ,  $\mu = \mu(T)$ . The governing equations are next made dimensionless.

## 2.2 NONDIMENSIONALIZED EQUATIONS

Dimensionless variables are used to nondimensionalize the governing equations as follows:

$$\bar{x} = \frac{x}{r^*} \quad (6a)$$

$$\bar{y} = \frac{y}{r^*} \quad (6b)$$

$$\bar{r} = \frac{r}{r^*} \quad (6c)$$

$$\bar{\rho} = \frac{\rho}{\rho_o} \quad (6d)$$

$$\bar{H} = \frac{H}{H_o} \quad (6e)$$

$$\bar{\mu} = \frac{\mu}{\mu_o} \quad (6f)$$

$$\bar{p} = \frac{p}{\left(\frac{\gamma}{\gamma-1}\right)^{\frac{1}{\gamma}} p_o} \quad (6g)$$

$$\bar{u} = \frac{u}{\left(H_o\right)^{\frac{1}{\gamma}}} \quad (6h)$$

$$\bar{v} = \frac{v}{\left(H_o\right)^{\frac{1}{\gamma}}} \quad (6i)$$

Using these equations in Eqs. (1) through (3) gives for the continuity, momentum, and total energy equation, respectively,

$$\frac{\partial(\bar{\rho} \bar{r} \bar{u})}{\partial \bar{x}} + \frac{\partial(\bar{\rho} \bar{r} \bar{v})}{\partial \bar{y}} = 0 \quad (7)$$

$$\bar{\rho} \bar{u} \frac{\partial \bar{u}}{\partial \bar{x}} + \bar{\rho} \bar{v} \frac{\partial \bar{u}}{\partial \bar{y}} = - \frac{d\bar{p}}{d\bar{x}} - \frac{(2)^{1/2}}{Re_{o,r^*}} \frac{1}{\bar{r}} \frac{\partial}{\partial \bar{y}} \left( \bar{r} \bar{\mu} \frac{\partial \bar{u}}{\partial \bar{y}} \right) \quad (8)$$

and

$$\bar{\rho} \bar{u} \frac{\partial \bar{H}}{\partial \bar{x}} + \bar{\rho} \bar{v} \frac{\partial \bar{H}}{\partial \bar{y}} = \frac{(2)^{1/2}}{Re_{o,r^*}} \frac{1}{\bar{r}} \frac{\partial}{\partial \bar{y}} \left\{ \bar{r} \left[ \frac{\bar{\mu}}{Pr} \frac{\partial \bar{H}}{\partial \bar{y}} + \bar{\mu} \left( 1 - \frac{1}{Pr} \right) \bar{u} \frac{\partial \bar{u}}{\partial \bar{y}} \right] \right\} \quad (9)$$

where

$$Re_{o,r^*} = \frac{\rho_o (2H_o)^{1/2} r^*}{\mu_o} \quad (10)$$

A few comments are in order concerning the choice of the dimensionless variables. Note that  $(H_o)^{1/2}$  was used to normalize the velocity components  $u$  and  $v$  instead of the more commonly used maximum velocity  $(2H_o)^{1/2}$ . The motivation for this was to recover the same form of the boundary-layer equations in dimensionless variables as in physical plane variables. If  $(2H_o)^{1/2}$  were used in Eqs. (6h) and (6i) in place of  $(H_o)^{1/2}$ , then the term  $\bar{\mu} [1 - (1/Pr)] \bar{u} \partial \bar{u} / \partial \bar{y}$  in the right hand side of Eq. (9) would be  $2\bar{\mu} [1 - (1/Pr)] \bar{u} \partial \bar{u} / \partial \bar{y}$ , which would not be the same as in Eq. (3). The maximum velocity  $(2H_o)^{1/2}$  was used in the definition of  $Re_{o,r^*}$  for convenience. This introduces the term  $(2)^{-1/2}$  as a coefficient of  $Re_{o,r^*}$ , but since  $Re_{o,r^*}$  is a constant for each solution, the constant  $(2)^{-1/2}$  causes no inconveniences in the numerical solutions. Note that by defining a new viscosity,  $\mu = (2)^{1/2} \bar{\mu} / Re_{o,r^*}$ , Eqs. (7) through (9) are identical to Eqs. (1) through (3). This, in fact, was done in the numerical computations.

For a given set of initial conditions, boundary conditions,  $\gamma$ ,  $Pr$ , nozzle geometry, etc., the solution to Eqs. (7) through (9) depends only on  $Re_{o,r^*}$  if a power law viscosity variation with temperature is assumed, i.e.,  $\bar{\mu} = \bar{T}^\xi = (T/T_o)^\xi$ . However, if, for example, Sutherland's viscosity law is assumed, then the solutions will also depend on the absolute value of temperature. Because the calculation of



viscosity is carried out in a separate subroutine in the computer program, it is convenient to use any viscosity law desired. Solutions will be presented for both Sutherland's law and power law variations of viscosity.

## 2.3 TRANSFORMED EQUATIONS

Equations (7) through (9) were transformed from the dimensionless physical  $\bar{x} - \bar{y}$  plane to the  $\xi - \omega$  plane by the transformation variables

$$\xi(\bar{x}) = \bar{x} \quad (11)$$

and

$$\omega(\bar{x}, \bar{y}) = \frac{\psi(\bar{x}, \bar{y}) - \psi_I(\bar{x})}{\psi_E(\bar{x}) - \psi_I(\bar{x})} \quad (12)$$

where  $\psi(\bar{x}, \bar{y})$  is the stream function which identically satisfies the continuity equation, Eq. (7), i. e.,

$$\frac{\partial \psi}{\partial \bar{x}} = -\bar{\rho} \bar{v} \bar{r} \quad (13)$$

and

$$\frac{\partial \psi}{\partial \bar{y}} = \bar{\rho} \bar{u} \bar{r} \quad (14)$$

The transformation used is that due to von Mises with  $\omega$  introduced to restrict the integration across the boundary layer from zero to unity. The subscripts I and E denote the inner and outer edge of the boundary layer, respectively, and  $\psi_I$  and  $\psi_E$  are functions of  $\bar{x}$  only. The operators  $(\partial/\partial \bar{x})$  and  $(\partial/\partial \bar{y})$  are given by

$$\frac{\partial}{\partial \bar{x}} = \frac{\partial}{\partial \xi} + \frac{\partial \omega}{\partial \bar{x}} \frac{\partial}{\partial \omega} = \frac{\partial}{\partial \xi} + \left( \frac{\partial \omega}{\partial \psi} \frac{\partial \psi}{\partial \bar{x}} + \frac{\partial \omega}{\partial \psi_I} \frac{d\psi_I}{d\bar{x}} + \frac{\partial \omega}{\partial \psi_E} \frac{d\psi_E}{d\bar{x}} \right) \frac{\partial}{\partial \omega} \quad (15)$$

and

$$\frac{\partial}{\partial \bar{y}} = \frac{\partial \omega}{\partial \bar{y}} \frac{\partial}{\partial \omega} = \frac{\partial \omega}{\partial \psi} \frac{\partial \psi}{\partial \bar{y}} \frac{\partial}{\partial \omega} \quad (16)$$

Using Eqs. (12) through (14) in Eqs. (15) and (16) and applying them to Eqs. (8) and (9) give for the momentum and total energy equations

$$\frac{\partial \bar{u}}{\partial \bar{x}} + \frac{\bar{r}_I \dot{m}_I + \omega(\bar{r}_E \dot{m}_E - \bar{r}_I \dot{m}_I)}{\psi_E - \psi_I} \frac{\partial \bar{u}}{\partial \omega} = \frac{(2)^{1/2}}{Re_{o,r^*}} \frac{\partial}{\partial \omega} \left[ \frac{\bar{r}^2 \bar{\rho} \bar{u} \bar{\mu}}{(\psi_E - \psi_I)^2} \frac{\partial \bar{u}}{\partial \omega} \right] - \frac{1}{\bar{\rho} \bar{u}} \frac{d\bar{p}}{d\bar{x}} \quad (17)$$

and

$$\begin{aligned} \frac{\partial \bar{H}}{\partial \bar{x}} + \frac{\bar{r}_I \dot{m}_I + \omega(\bar{r}_E \dot{m}_E - \bar{r}_I \dot{m}_I)}{\psi_E - \psi_I} \frac{\partial \bar{H}}{\partial \omega} = \frac{(2)^{1/2}}{Re_{o,r^*}} \left\{ \frac{\partial}{\partial \omega} \left[ \frac{\bar{r}^2 \bar{\rho} \bar{u} \bar{\mu}}{(\psi_E - \psi_I)^2} \frac{\partial \bar{H}}{\partial \omega} \right] \right. \\ \left. + \frac{\partial}{\partial \omega} \left[ \frac{\bar{r}^2 \bar{\rho} \bar{u} \bar{\mu}}{(\psi_E - \psi_I)^2} \left( 1 - \frac{1}{Pr} \right) \frac{\partial (\bar{u}^2/2)}{\partial \omega} \right] \right\} \end{aligned} \quad (18)$$

where

$$\frac{d\psi_I}{d\bar{x}} = -\bar{r}_I \dot{m}_I \quad (19)$$

and

$$\frac{d\psi_E}{d\bar{x}} = -\bar{r}_E \dot{m}_E \quad (20)$$

and where  $\xi(\bar{x})$  has been replaced by  $\bar{x}$ . Except for the constant  $(2)^{1/2}/Re_{o,r^*}$ , Eqs. (17) and (18) are identical to the momentum and total energy equations for external flow which are solved numerically by the method of Patankar and Spalding (Ref. 11). The calculation of the mass transfer fluxes  $\dot{m}_I$  and  $\dot{m}_E$  will be discussed in Section III.

The boundary-layer displacement thickness was used to calculate an effective nozzle geometry which in turn was used to calculate an axial pressure distribution. The displacement thickness,  $\delta^*$ , which takes into account transverse curvature is expressed by Probstein and Elliott (Ref. 12) as

$$\int_0^{\delta^*} 2\pi r \rho_E u_E dy = \int_0^{y_E} 2\pi r (\rho_E u_E - \rho u) dy \quad (21)$$

Solving Eq. (21) for  $\delta^*$  gives

$$\frac{\delta^*}{r^*} = \frac{\bar{r}_w - \left[ \bar{r}_w^2 - 2 \cos \alpha \left( \bar{y}_E \bar{r}_w - \frac{\bar{y}_E^2 \cos \alpha}{2} - \frac{\psi_E - \psi_I}{\bar{\rho}_E \bar{u}_E} \right) \right]^{1/2}}{\cos \alpha} \quad (22)$$

A quadratic equation for  $\delta^*$  must be solved to obtain Eq. (22) from Eq. (21). The positive sign was chosen so that  $\delta^*/r^* < \bar{r}_w/\cos \alpha$ . The displacement thicknesses for axisymmetric flows without transverse curvature and planar flows can be obtained by using  $(r_w)^\nu$  in place of  $r$  in Eq. (21). The displacement thicknesses are then given by

$$\frac{\delta^*}{r^*} = \bar{y}_E - \frac{(\psi_E - \psi_I)}{(\bar{r}_w)^\nu \bar{\rho}_E \bar{u}_E} \quad (23)$$

where  $\nu = 0$  for planar flows and  $\nu = 1$  for axisymmetric flows without transverse curvature.

### SECTION III NUMERICAL SOLUTION

The numerical solution of Eqs. (17) and (18) is discussed in this section. The basic scheme is briefly described and a listing of the computer code is presented. A description of the necessary inputs to the program is given, and some computational difficulties which have been encountered with the program are discussed.

#### 3.1 BASIC SCHEME

As previously stated, the basic numerical integration scheme of Patankar and Spalding (Ref. 11) was suitably modified and used to solve the governing internal flow equations pertinent to the present investigation. Because the flow regime of the present investigation was entirely laminar, some subroutines of the computer code listed in Ref. 11 which were associated with turbulent flow were removed for the present code. Also, most, but not all, statements pertaining to turbulent flow were removed. The computer code as used for the present investigation is

listed in Appendix III. Essentially this same program was used on two different computers at AEDC, a Scientific Data Systems (SDS) 9300 and an International Business Machines (IBM) 370/155. The code in Appendix III is the one used on the IBM 370/155.

The basic numerical scheme used by Patankar and Spalding is discussed in detail in Ref. 11. One of the primary features of this finite difference technique is that the set of linear algebraic equations which must be solved has only three unknowns in each equation, and this set can be solved by simple successive substitution (Gauss reduction, or elimination, Ref. 13) rather than by matrix inversion. This technique provides a saving in computational time. For example, the time required to solve the algebraic equations by elimination (at a fixed  $\bar{x}$  location) is proportional to the number of unknowns, whereas the time required to solve the equations by matrix inversion is proportional to the square of the number of unknowns (Ref. 13). On the IBM 370/155, a solution at a fixed  $\bar{x}$  location required approximately 0.6 sec using 200 grid points across the boundary layer ( $w$  direction) in single precision. The corresponding time required on the SDS 9300 was approximately 10 sec. The IBM 370/155 carried 8 digits in single precision, whereas the SDS 9300 carried 12.

The general method of solution consisted of matching the inviscid and viscous flow regions in the nozzle by iterating on the axial pressure distribution. An initial guess of the axial pressure distribution throughout the nozzle is made, and a solution is obtained. The displacement thickness calculated in this solution is used to obtain an effective nozzle geometry which in turn is used to calculate a new pressure distribution from one-dimensional, perfect gas, expansion theory. A typical iteration and convergence process is illustrated in Fig. 2. The use of one-dimensional perfect gas expansion theory as opposed to a method-of-characteristics solution, for example, seems justified on the basis of the agreement with experimental data in Section V. The same iteration process as used here and some suggestions for choosing the initial pressure distribution are discussed further by Whitfield and Lewis (Ref. 5).

The symbols and subroutines used in the Patankar and Spalding code are clearly defined and discussed in Ref. 11. Therefore, the remainder of this section is directed toward the modifications and additions which have been made to the code of Ref. 11.

### 3.2 INPUT CONDITIONS

The input requirements to this program are particularly simple. The input was modified somewhat from that of the original code (Ref. 11), and the input variables are described below in the order they are read-in in the present code (Appendix III).

SYMBOL	DESCRIPTION
KRAD	This input permits the treatment of plane flows and axisymmetric flows with first-order transverse curvature. Also, although not pointed out in Ref. 11, axisymmetric flows without transverse curvature can be treated by setting $KRAD = 0$ . Plane flows can be treated by setting $KRAD = 0$ and $\bar{r}_w(\bar{x}) \equiv 1$ (or a constant). Axisymmetric flows including first-order transverse curvature are treated by setting $KRAD = 1$ (at least not zero) and using the actual geometry $\bar{r}_w(\bar{x})$ .
IDIMEN	If the nozzle considered is two-dimensional, set $IDIMEN = 0$ . This sets $\bar{r}_w(\bar{x}) \equiv 1$ in subroutine RAD. If the nozzle considered is axisymmetric set $IDIMEN = 1$ .
NEQ	This is the number of partial differential equations to be solved. The code of Ref. 11 also includes the solution to the equation for the conservation of chemical species. However, this equation was never considered in this investigation and only the momentum and total energy equations were used, in which case $NEQ = 2$ . The chemical species equation is, however, retained in the present code.
KEX	This input specifies the type of E boundary. It can be either 1, 2, or 3, according to whether the E boundary is a wall, free boundary, or a symmetry line, respectively. However, in the present investigation KEX was always 2, i. e., E was a free boundary, and certain modifications must be made to the present code if anything other than $KEX = 2$ is used.

KIN	This is similar to KEX except KIN specified the type of I boundary. For the present code KIN = 1 must be used; otherwise certain modifications must be made.
IHEAT	This is used in subroutine FBC and indicates a wall temperature boundary condition if IHEAT = 1 and a wall heat-transfer rate if IHEAT $\neq$ 1. In the present code, the only wall heat flux considered was zero, i. e., an adiabatic wall. If a heat flux other than zero is prescribed, then a few statements in subroutine SLIP must be modified (see Ref. 11). The only wall temperature distribution considered in the present work was $T_w/T_o = \text{constant}$ . However, subroutine FBC is easily modified to accommodate any desired variation of $T_w$ .
N	This is the number of strips across the boundary layer, i. e., in the $\omega$ direction. It must always be at least three less than the dimensions of the arrays of the variables across the layer, e. g., the maximum N which can be used with the dimensions of the arrays in the present code is 197.
REØRS	Reservoir Reynolds number, $Re_{o,r}^*$ .
ZETA	Exponent in the power law variation of viscosity with temperature, $\mu \sim T^\zeta$
PR(1)	Prandtl number, Pr
GAM	Ratio of specific heats, $\gamma$
ALPHA	Nozzle wall half-angle, $\alpha$
XR	Longitudinal radius of curvature of the nozzle upstream of the throat, $\bar{R}$
XL	Termination condition for the computations, maximum value of $\bar{x}$
USUP	This input controls the location of the E boundary. It is associated with the entrainment rate and it will be discussed in the following subsection. USUP was varied from 0.99 to 0.999, and was usually 0.995.

YSTART	Initial velocity and total enthalpy profiles were calculated from the expressions $u/u_E = 2\eta - \eta^2$ and $H/H_O = H_w/H_O + [1 - (H_w/H_O)]u/u_E$ where $\eta = \bar{y}/\bar{y}_E$ and $\bar{y}_E = \text{YSTART}$ . Suggestions for choosing YSTART will be given in the following subsection. A typical value of YSTART is 0.5.
TWTØ	Ratio of wall to total temperature, $T_w/T_O$
XSTEP	Specification of the integration step-size in the $\bar{x}$ direction in terms of local wall radius, e.g., step size, DX, is given by the product of XSTEP times $\bar{r}_w$ . A typical value of XSTEP is 0.05.
LMAX	Number of $\bar{x}$ locations where an input pressure is specified.
XX(L)	Array of $\bar{x}$ locations where an input pressure is specified. Array goes from 1 to LMAX.
POP(L)	Input pressure for corresponding $\bar{x}$ location, XX(L). Array goes from 1 to LMAX.

The last three inputs, LMAX, XX(L), and POP(L), are read-in in subroutine PRE, the other inputs are read-in in subroutine BEGIN.

Because of the nature of the process involved in iterating on the axial pressure distribution, it is important to input a smooth initial pressure distribution. For the present computations, the initial pressure distribution was calculated using the actual geometry at and upstream of the throat and some effective inviscid nozzle wall downstream of the throat. (Actually, the slope of the assumed inviscid nozzle wall just downstream of the throat was matched to the nozzle wall half-angle to produce a smooth wall in order to have a smooth pressure distribution.) The simple program used to calculate the initial pressure distribution for the present computations is included in Appendix IV for convenience of users where such an approximation is adequate. The particular version of the code presented in Appendix IV uses  $\delta^* \sim x^{3/2}$  for axisymmetric nozzles and  $\delta^* \sim x$  for two-dimensional nozzles. Although  $\delta^* \sim x^{3/2}$  was not used to calculate the initial pressure distribution for all axisymmetric nozzle computations presented herein, it appears to provide a reasonable approximation to the variation of  $\delta^*$  in axisymmetric nozzles.

Inasmuch as several wind tunnel and laser nozzles have conical sections downstream of the throat and constant longitudinal radius of curvature for the upstream converging portions, this general nozzle geometry (which can be sufficiently described by the inputs ALPHA and XR) was considered in this investigation. However, subroutine RAD can be easily modified to include any geometry, such as for example contoured nozzles which were analyzed in Ref. 5 using the same governing equations as used here.

### 3.3 SOME POSSIBLE COMPUTATIONAL DIFFICULTIES

The mass-transfer rate, or entrainment rate, across the E boundary essentially governs the location of the edge of the boundary layer. This technique of locating the edge of the boundary layer has certain advantages in analyzing low-density nozzle flows; however, it might also cause some difficulties if not handled correctly. The entrainment rate was calculated in the present investigation by evaluating the momentum equation, Eq. (17), along a constant  $\omega$  line, denoted as  $\omega_B$ , near the E boundary. This technique is discussed in Ref. 11. The scheme requires the specification of the velocity along  $\omega = \omega_B$  (where  $\omega_B$  was taken as 0.9) at the next downstream station. This velocity is denoted as  $\tilde{u}_B$  and it is suggested in Ref. 11 that it be taken as  $\tilde{u}_B = 0.99 \bar{u}_E$ , where  $\bar{u}_E$  is the velocity at the edge of the boundary layer at the next downstream station. (Note that  $\bar{u}_E$  can be calculated from the Euler equation since  $d\bar{p}/d\bar{x}$  is presumed known for the particular iteration.) It was found in the present work, however, that more flexibility could be obtained with the program if  $\tilde{u}_B$  was taken as  $\tilde{u}_B = (\text{USUP})\bar{u}_E$  and USUP was input for each solution. The quantity USUP provides a means of suppressing the outer edge of the boundary layer which is advantageous in treating flows which are nearly merged. For example, during the process of iterating on the axial pressure distribution, it was observed (Fig. 2, and also Ref. 5) that  $\delta^*$  resulting from the first two iterations usually provided upper and lower bounds on the final converged  $\delta^*$ . Therefore, if the flow is sufficiently rarefied, the pressure distribution resulting from the thinnest  $\delta^*$  may be such that the following iteration would predict a merged flow when in fact the flow is not merged and could be calculated if a better guess for the initial pressure distribution could be made. In some cases the calculation of merged flow in the iteration process can be avoided by using a small value of USUP (a value of 0.99 is herein regarded as small and 0.999 is regarded as large) to suppress the edge of the boundary layer and prevent an indication of merging. The suppression seems to



apply only to the outer edge of the layer and the calculated profiles over most of the layer remain essentially unchanged. For this reason, the converged  $\delta^*$ , or pressure distribution, obtained using a small USUP usually differs by a small amount from that obtained using a larger USUP, say 0.995. After convergence is obtained using a small value of USUP a final solution can be obtained using a larger value. The value of 0.99 for  $\tilde{u}_B/\bar{u}_E$  as suggested in Ref. 11 seems to excessively suppress the boundary layer for the present internal flow calculations. For most solutions reported herein, USUP was 0.995.

The step-size along the  $\bar{x}$  component was taken for most of the solutions as 5 or 7.5 percent of the local wall radius. This step-size was sufficiently small for most problems. However, if calculations of properties in the nozzle throat region are of particular interest, such as the nozzle wall heat-transfer rate, a smaller step-size may be desirable.

In some applications where nozzle exit properties are of particular interest, it may be desirable to conserve computer time and use a relatively large  $\bar{x}$  component step-size. For such problems some difficulties might be encountered in starting the solutions. Consider a finite-difference form of Eqs. (19) and (20)

$$(\psi_E - \psi_I)_D = (\psi_E - \psi_I)_U + (\bar{r}_I \dot{m}_I - \bar{r}_E \dot{m}_E)_U (\bar{x}_D - \bar{x}_U) \quad (24)$$

If  $Re_0$ ,  $r^*$  and/or YSTART is small, then  $(\psi_E - \psi_I)_U$  calculated from the initial profile will be small. Depending on the initial profiles and flow conditions,  $\dot{m}_E$  may be positive for the first few stations and therefore  $(\psi_E - \psi_I)_D$  could be less than  $(\psi_E - \psi_I)_U$  for these first few stations and might even become negative. To circumvent this difficulty one could reduce the step-size  $(\bar{x}_D - \bar{x}_U)$ . However, if this is not desirable in view of computational time requirements, another approach is to increase YSTART in order to increase  $(\psi_E - \psi_I)_U$  at the first station. The first few station solutions would consequently not be as accurate as solutions obtained by using a small  $\bar{x}$  step-size. Therefore, although the solutions are started at the beginning of the converging portion of the nozzle upstream of the throat, this technique of increasing YSTART should be used with caution if accurate solutions (particularly properties which depend on derivatives near the wall such as heat-transfer rate) in the throat region are required. As stated previously, a typical value of YSTART was 0.5. The largest value of YSTART used to obtain solutions was unity, but this depends on XR.

Heat transfer and viscous effects change the effective nozzle throat from the location corresponding to the actual geometric nozzle throat. The subroutine NEWPPØ searches for the minimum effective nozzle radius and uses it for the throat in calculating a one-dimensional pressure distribution for the next iteration. However, if a sufficient number of solutions near the throat are not taken, then the true minimum area and its location used in calculating a new pressure distribution may not be accurately approximated. Then, the resulting  $d\bar{p}/d\bar{x}$  in the throat region for the following iteration may not be smooth. In this case, the error in  $d\bar{p}/d\bar{x}$  for each successive iteration would become worse. This is especially a problem in solutions for flows which have adiabatic or relatively hot nozzle walls. It is suggested that if the initial guess of the  $\delta^*$  distribution is not a particularly good one, e.g., if the calculated  $\delta^*$  at the exit is not within 20 to 30 percent of the assumed  $\delta^*$ , then an improved pressure distribution should be calculated by the program in Appendix IV (or some similar method). This ensures a smooth pressure distribution, and since convergence is, in general, much faster in the throat region than further downstream where the relative displacement thicknesses are larger, few, if any, extra iterations are required.

Although areas have been pointed out where computational difficulties have been encountered with this program, it should also be pointed out that this numerical scheme is actually rather rugged, as for example compared to the method of Ref. 5. It is in general not sensitive to input conditions and seldom "blows up."

#### SECTION IV NUMERICAL RESULTS

Solutions are presented in this section for typical nozzle configurations which provide some indication of the effect of  $Re_{O,r^*}$ ,  $\gamma$ ,  $Pr$ ,  $\xi$ ,  $T_w/T_o$ ,  $\alpha$ , transverse curvature, and two-dimensional versus axisymmetric flows. Table I (Appendix II) summarizes the conditions of the solutions presented in this section.

Of particular interest in nozzle flows is the displacement thickness,  $\delta^*$ . By using  $\delta^*$  and the nozzle geometry, an effective inviscid nozzle radius can be determined from which Mach number and other flow properties outside the boundary layer can be estimated. The displacement thicknesses for Conditions 1 to 8 of Table I are presented in Figs. 3 to 10.

Solutions were started at the beginning of the converging portion of the nozzles where  $z/r^* = -3$ . However, to conserve computing time, extremely small step-sizes were not utilized for all the solutions in this region (as discussed in Section III), and results are not presented in Figs. 3 to 10 for  $z/r^* < -2$ . Some solutions were repeated, however, with smaller step-sizes with no appreciable changes in the results presented.

At least for some values of  $Re_{O,r^*}$  in Figs. 3 to 7 and 9 to 10, negative displacement thicknesses were calculated in the throat region. This is due to the relatively cool wall increasing the gas density and hence the local mass flux near the wall. The adiabatic wall results presented in Fig. 8 do not indicate negative  $\delta^*$  for the same flow conditions. Similar results concerning the calculation of negative  $\delta^*$  have been reported previously, e. g., Potter and Carden (Ref. 3) and Whitfield and Lewis (Refs. 4 and 5).

Some indication of the effect of using various gases in a fixed nozzle geometry with fixed flow conditions is provided in Figs. 3 to 5. The specific heat ratio, Prandtl number, and power law viscosity variation with temperature of Figs. 3 to 5 closely approximate the properties of carbon dioxide ( $CO_2$ ), helium (He), and nitrogen ( $N_2$ ), respectively. For example, by considering the nozzle exit displacement thickness for  $Re_{O,r^*} = 10^4$ , one observes that, for the indicated flow conditions,  $\delta^*$  using He is about 200 percent of that when using  $CO_2$ , and  $\delta^*$  using  $N_2$  is about 150 percent of that when using  $CO_2$ .

Results are presented in Figs. 5 and 6 for identical conditions except for the nozzle wall half-angle. Figure 5 has a wall half-angle of 10-deg, and Fig. 6 has a half-angle of 15 deg. For the same geometric area ratio, the expansion process is more rapid for the  $\alpha = 15$  deg nozzle than the  $\alpha = 10$  deg. Also, the nozzle wall length for the same area ratio is longer for the 10-deg nozzle than for the 15-deg nozzle. The result is to produce a larger exit  $\delta^*$  for the 10-deg nozzle than for the 15-deg nozzle for the same geometric area ratio. For  $Re_{O,r^*} = 3 \times 10^3$ , the 10-deg nozzle exit  $\delta^*$  is about 18 percent larger than that of the 15-deg nozzle.

It should be pointed out that although  $\delta^*$  is relatively small because of the cool walls,  $\delta$  is not necessarily small. For example, in Fig. 5 for  $Re_{O,r^*} = 10^3$ , the flow merges (i. e., the boundary layer completely fills the nozzle) at a point where  $\delta/r^* \approx 3$ . For these conditions,  $\delta^*/\delta \sim 0(1/10)$ . The ratio  $\delta^*/\delta$  tends to increase with wall temperature.

In general, the wall temperature seems to have a stronger effect on  $\delta^*$  than on  $\delta$  (Ref. 4). In Figs. 5, 7, and 8 the effect of nozzle wall temperature was investigated, with other conditions held constant, by considering  $T_w/T_0 = 1/10$ ,  $T_w/T_0 = 1/3$ , and an adiabatic wall. For  $Re_{O,r}^* = 10^4$ , the ratio  $\delta^*/\delta$  at the nozzle exit was 0.30, 0.48, and 0.68, respectively.

The effect of Prandtl number was investigated by repeating the conditions of Fig. 5 but with  $Pr = 1$  in place of  $5/7$ . The results are presented in Fig. 9. The displacement thickness was found to increase for  $Pr = 1$  by approximately 20 percent at the nozzle exit.

The conditions of Fig. 5 were also repeated using  $\xi = 1$  in place of  $\xi = 2/3$  to investigate the effect of the power law variation of viscosity with temperature. For  $\xi = 1$  the displacement thickness was found to decrease by 20 to 25 percent below that for  $\xi = 2/3$  (see Figs. 5 and 10). Note that, since  $\bar{\mu} = \bar{T}^\xi$  and  $\bar{T} \leq 1$ , then the flow is more viscous for  $\xi = 2/3$  than for  $\xi = 1$ .

Velocity and temperature profiles calculated with and without transverse curvature terms are presented in Fig. 11 for Conditions 3 and 9 (Table I) with  $Re_{O,r}^* = 3 \times 10^3$ . Neglecting transverse curvature decreases the boundary-layer thickness for internal flow. The effect of transverse curvature is negligible for thin boundary layers, but may be significant for thick boundary layers. Further results and discussion concerning the effects of transverse curvature are reported in Ref. 5.

The displacement thicknesses of an axisymmetric and two-dimensional nozzle are presented in Fig. 12. For each nozzle,  $A_e/A^* = 5$ , and therefore, the two-dimensional nozzle is considerably longer since  $\alpha = 10$  deg for each. The result is to produce a significantly larger displacement thickness for the two-dimensional nozzle than for the axisymmetric nozzle.

## SECTION V COMPARISONS WITH EXPERIMENTAL DATA AND OTHER THEORETICAL RESULTS

Curves of  $Re_{O,r}^*/(p_0 r^*)$  versus total temperature for various gases are presented in Fig. 13 for the convenience of determining  $Re_{O,r}^*$ . The viscosities used for all gases in Fig. 13 except carbon dioxide ( $CO_2$ ) are

those given by Svehla (Ref. 14). The viscosity of  $\text{CO}_2$  was taken from Table 8.4-2 of Hirschfelder, Curtiss, and Bird (Ref. 15).

Highly viscous nozzle flows are usually associated with nozzles of small physical size. The spatial resolution of experimental measurements in such nozzles is obviously restricted. However, highly viscous flows can also be produced in large nozzles if sufficiently large volume flows can be pumped at low pressures, thereby permitting more detailed investigations of the boundary layer. Such investigations are possible in the Aerospace Research Chamber 10V in the VKF at AEDC. The present and some previous calculation methods will be compared with experimental data taken in Chamber 10V using a nominal Mach three nozzle, denoted M3 nozzle. This is a 10-deg half-angle conical nozzle with  $d^* = 27$  cm,  $d_e = 76.2$  cm, and  $R = 11.2$  cm. The walls of this nozzle were cooled with liquid nitrogen to maintain a constant nozzle wall temperature of about 85°K.

Calculated and measured pitot pressure profiles at the nozzle throat are presented in Fig. 14. Nitrogen was the test gas used for these and all other experimental data presented in this report. The present results are in good agreement with the results using the method of Ref. 5. The calculated profiles are in relatively good agreement with the measured profile for these conditions.

Calculated and measured pitot pressure profiles at the nozzle exit are presented in Fig. 15. This calculation was performed using  $\xi = 2/3$ , whereas some other results presented herein, e.g., Fig. 14, were obtained using Sutherland's viscosity law for nitrogen. However, over the temperature range of the experimental data taken in Chamber 10V, there was negligible difference in the results using either viscosity variation with temperature.

Present calculations are compared to calculations by the method of Rae (Ref. 10) and experimental data in Figs. 16 and 17. The present results are in relatively good agreement with the experimental data, but Rae's method is found to overestimate the size of the viscous region for these conditions. Results were also presented in Ref. 5 for the conditions of Fig. 17. The calculated profile from Ref. 5 is almost identical with the present result in Fig. 17 (see Ref. 5) and is not presented.

Pitot pressure profiles at about 7 throat radii downstream of the M3 nozzle throat are presented in Fig. 18 for  $\text{Re}_{O,r^*} = 1170$ . A relative minimum exists at the nozzle centerline in the experimentally

measured profile, and slight "humps" or relative maximums exist near the edge of the boundary layer. It should be pointed out that the existence of humps does not necessarily imply that the flow is non-isentropic. Imagine a radial pitot pressure profile in an inviscid contoured supersonic nozzle which is sufficiently far downstream of the throat to pass through a portion of the uniform parallel flow near the centerline. Such a pitot profile would have lower values near the nozzle centerline than near the wall because of the larger Mach numbers near the centerline. However, the matching of such an inviscid flow with a realistic viscous flow requires the pitot pressure near the wall to approach the local static pressure which is less than the centerline pitot pressure. Therefore, it is not difficult to conceive of humps in such a radial pitot profile because of the matching of inviscid and viscous flow. This argument is based on flow in a contoured nozzle. It is applied to the present case because the displacement thickness effectively contours the nozzle. A more accurate approach of investigating such flows would be to remove the present assumption of one-dimensional inviscid flow outside the boundary layer and obtain more accurate solutions, such as, inviscid method-of-characteristics solutions. However, the pitot pressure profile is relatively well predicted in Fig. 18, and for this work, the assumption of one-dimensional inviscid flow outside the boundary layer is considered acceptable.

Just as radial pitot profiles with humps do not necessarily imply that the flow is non-isentropic, a flat radial profile does not necessarily imply that the flow is isentropic. Consider the pitot pressure data in Fig. 19. Both the calculated and measured profiles are relatively flat for  $y/r_w$  larger than about 0.7. However, in this case the pitot profile is not a good measure of the extent of the nozzle wall viscous effects as shown in Fig. 20. From Fig. 20, the boundary-layer thickness as estimated from the pitot profile is about 55 percent of the nozzle radius, whereas it is calculated to be actually over 80 percent. The pitot profile for the case in Fig. 20 implies that 20 percent of the cross-sectional area of the nozzle at this point is core flow, whereas actually less than 4 percent is core flow. The reason a pitot profile might lead one astray is associated with the temperature or thermal boundary layer since pitot pressure depends, among other things, on  $u/(T)^{1/2}$ . The velocity variation is usually well behaved and fairly accurately predicted by simple analytical expressions based on boundary-layer thickness (Ref. 4); however, this is not the case with the thermal boundary layer. The temperature variation depends not only on local wall and edge values and gradients but also on the upstream conditions.

Therefore, some consideration should be given to the temperature variation in order to place limits-of-confidence on the use of pitot pressure as an indication of the nozzle wall viscous effects.

Carden (Ref. 16) measured local heat-transfer coefficients in an axisymmetric nozzle for  $Re_{O,r^*} = 5 \times 10^3$ . The experimental data were compared with calculated heat-transfer coefficients in Refs. 5 and 16. However, Whitfield made a mistake in Ref. 5 and presented solutions for  $r^* = 0.262$  cm instead of  $d^* = 0.262$  cm (0.103 in.) which corresponds to the actual nozzle throat dimension. Because of this error, the calculated heat-transfer coefficients (Ref. 5) from the iterated solutions were significantly below the experimental data of Carden (Ref. 16). Heat-transfer coefficients were calculated using the present method but with the inappropriate throat dimension of  $r^* = 0.262$  cm, and good agreement was obtained with the calculated results of Ref. 5. Results were also obtained with the present method using the proper throat dimension of  $d^* = 0.262$  cm, and good agreement with the experimental data was obtained as shown in Fig. 21. Also, in Fig. 21 are results from two of the methods Carden (Ref. 16) used for calculating the heat-transfer coefficient and one solution from Ref. 5. Although the result from Ref. 5 which is presented in Fig. 21 was not iterated to include the higher-order displacement effect, the result was obtained using the pressure distribution corresponding to the proper nozzle geometry and, therefore, is included in Fig. 21. This result from Ref. 5 is in relatively good agreement with the present result. All calculation methods underestimate the most upstream uncorrected experimental data point in Fig. 21. However, Carden points out that radiation from the arc used to heat the gas could increase the total heat-transfer rate to this portion of the nozzle. No corrections for radiation heat transfer were made to the experimental data.

It might be pointed out that the heat-transfer rate printed out in the present program, denoted as  $AJI(1)$ , is equal to  $q_w/(\rho_o H_o^{3/2})$ . Although made dimensionless, the numerical scheme used in Ref. 11 to calculate  $AJI(1)$  is retained in the present code in subroutine WALL.

## SECTION VI CONCLUSIONS

The present results were shown to be in good agreement with results from the method of Ref. 5. Although it was noted during the present investigation that more axial stations were required using the

present program than that of Ref. 5 to obtain the same degree of accuracy (presumably this is due to the transformation variables used in Ref. 5, which are advantageous for thin boundary layers but disadvantageous for thick internal boundary layers), the present program is much smaller, faster and easier to use. Comparisons with results from Rae's method (Ref. 10) and experimental data indicated the present method to be more accurate than Rae's for the conditions considered. It should be remembered, however, that the present work is not applicable to merged flows without modification, whereas Rae's method is more applicable to merged flows.

Consistent agreement was obtained between the present results and experimental data. Except for the heat-transfer data, the experimental data were taken in a relatively large nozzle where the boundary layer could be accurately probed. Similar agreement was obtained in Ref. 2 where extensive data were obtained in small nozzles,  $r^* \sim 0$  (0.1 cm). The numerical method used in Ref. 2 was developed by Mayne (Ref. 2), as stated previously, and differs from the original Patankar and Spalding method (Ref. 11) primarily in the numerical scheme near the wall.

The present method has not been modified for use in nozzle design; however, it is a straightforward matter to make such a modification (see Ref. 5). To design a nozzle, a new nozzle geometry,  $r_w(x)$ , is calculated from the displacement thickness from each iteration, and the new geometry is used for the next iteration while the desired axial pressure distribution is maintained for each iteration. It was found in Ref. 5 that convergence was, in general, more rapid in iterating on the nozzle geometry than on the axial pressure distribution.

## REFERENCES

1. Smithson, H. K., Price, L. L. and Whitfield, D. L. "Wind Tunnel Testing of Interactions of High Altitude Rocket Plumes with the Free Stream." AEDC-TR-71-118 (AD731141), September 1971.
2. Whitfield, D. L., Lewis, J. W. L., Williams, W. D., et. al. "Specie Number Density, Pitot Pressure, and Flow Visualization in the Near Field of Two Supersonic Nozzle Banks Used for Chemical Laser Systems." AEDC-TR-73-11, May 1973.



3. Potter, J. L. and Carden, W. H. "Design of Axisymmetric Contoured Nozzles for Laminar Hypersonic Flow." Journal of Spacecraft and Rockets, Vol. 5, No. 9, September 1968, pp. 1095-1100.
4. Whitfield, D. L. "Theoretical and Experimental Investigation of Boundary Layers in Low-Density Hypersonic Axisymmetric Nozzles." AEDC-TR-68-193 (AD674597), September 1968.
5. Whitfield, D. L. and Lewis, C. H. "Boundary-Layer Analysis of Low-Density Nozzles, Including Displacement, Slip, and Transverse Curvature." Journal of Spacecraft and Rockets, Vol. 7, No. 4, April 1970, pp. 462-468.
6. Cohen, C. B. and Reshotko, E. "Similar Solutions for the Compressible Laminar Boundary Layer with Heat Transfer and Pressure Gradient." NACA Report 1293, 1956.
7. Jaffe, N. A., Lind, R. C., and Smith, A. M. O. "Solution to the Binary Diffusion Laminar Boundary Layer Equations Including the Effect of Second-Order Transverse Curvature." AIAA Journal, Vol. 5, No. 9, September 1967, pp. 1563-1569.
8. Adams, J. C., Jr. "Similar Solutions for Viscous Compressible Laminar Flow in Slender Axisymmetric Channels." Ph. D. Dissertation, North Carolina State University, 1966.
9. Williams, J. C., III. "Conical Nozzle Flow with Velocity Slip and Temperature Jump." AIAA Journal, Vol. 5, No. 12, December 1967, pp. 2128-2134.
10. Rae, W. J. "Some Numerical Results on Viscous Low-Density Nozzle Flows in the Slender-Channel Approximation." AIAA Journal, Vol. 9, No. 5, May 1971, pp. 811-820.
11. Patankar, S. V. and Spalding, D. B. Heat and Mass Transfer in Boundary Layers. Morgan-Grampian: London 1967.
12. Probst, R. F. and Elliott, E. "The Transverse Curvature Effect in Compressible Axially Symmetric Laminar Boundary-Layer Flow." Journal of the Aeronautical Sciences, Vol. 23, No. 3, 1956, pp. 208-222.
13. Smith, G. D. Numerical Solution of Partial Differential Equations. Oxford University Press, New York, 1965.

14. Svehla, R. A. "Estimated Viscosities and Thermal Conductivities of Gases at High Temperatures." NASA TR-R-132, Washington, 1962.
15. Hirschfelder, J. O., Curtiss, C. F., and Bird, R. B. Molecular Theory of Gases and Liquids. John Wiley & Sons, Inc., New York, 1954.
16. Carden, W. H. "Local Heat-Transfer Coefficients in a Nozzle with High-Speed Laminar Flow." AIAA Journal, Vol. 3, No. 12, December 1965, pp. 2183-2188.
17. Beckwith, I. E. and Cohen, N. B. "Application of Similar Solutions to Calculation of Laminar Heat Transfer on Bodies with Yaw and Large Pressure Gradient in High-Speed Flow." NASA TND-625, 1961.
18. Pasqua, P. F., Stevens, P. N., Mott, J. E., Roland, H. C., and Robinson, J. C. "Analytical Studies on Nozzle Throat Cooling." AEDC-TDR-63-58 (AD400746), 1963.

**APPENDIXES**

- I. ILLUSTRATIONS**
- II. TABLE**
- III. BOUNDARY-LAYER COMPUTER CODE**
- IV. INITIAL PRESSURE DISTRIBUTION  
COMPUTER CODE**

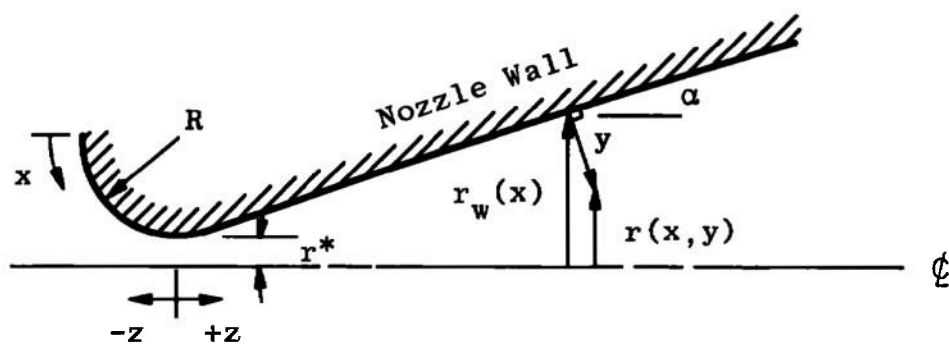


Fig. 1 Definition of Coordinate System

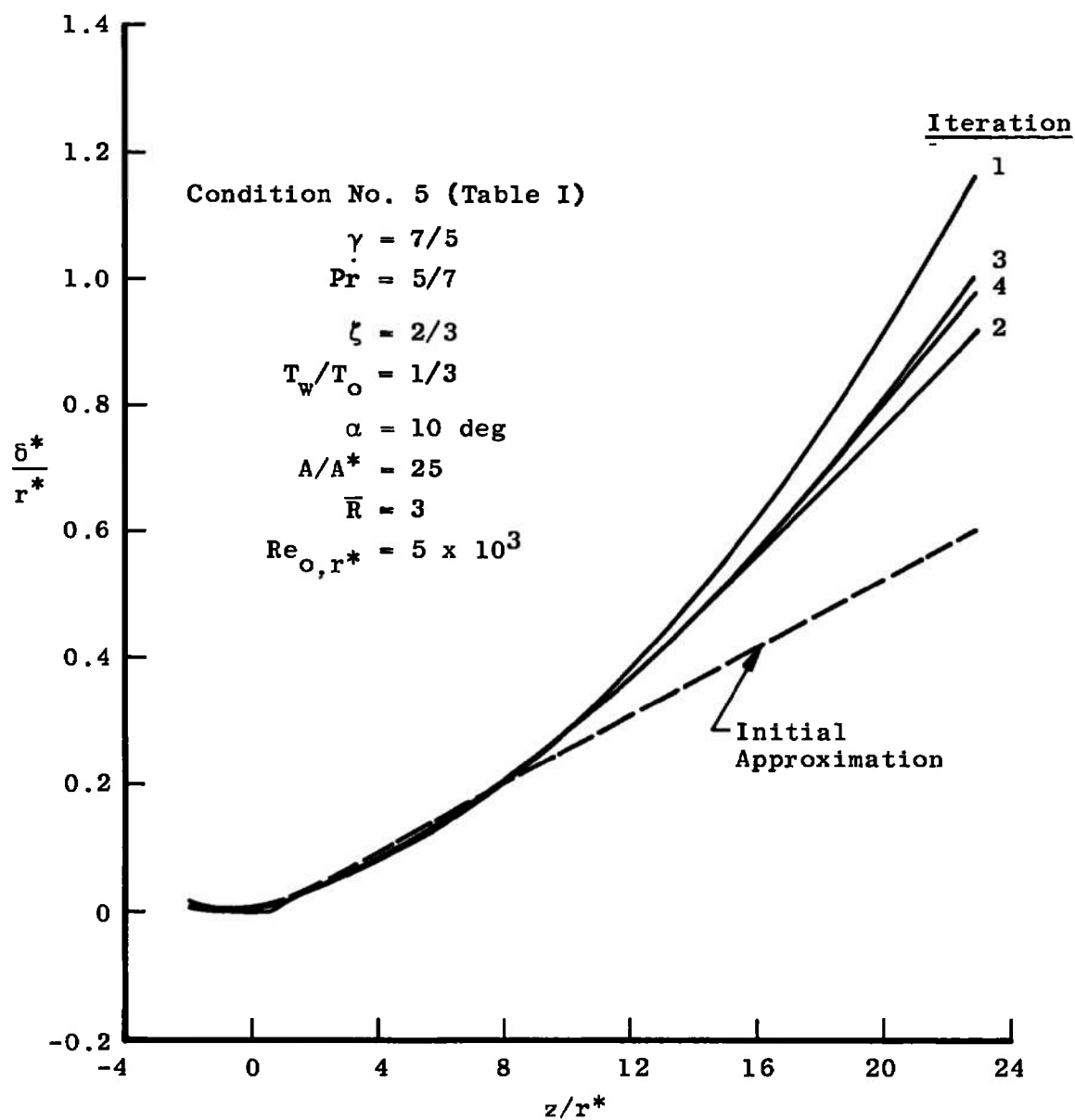


Fig. 2 Displacement Thickness of Successive Iterations  
for Condition No. 5 (Table I)

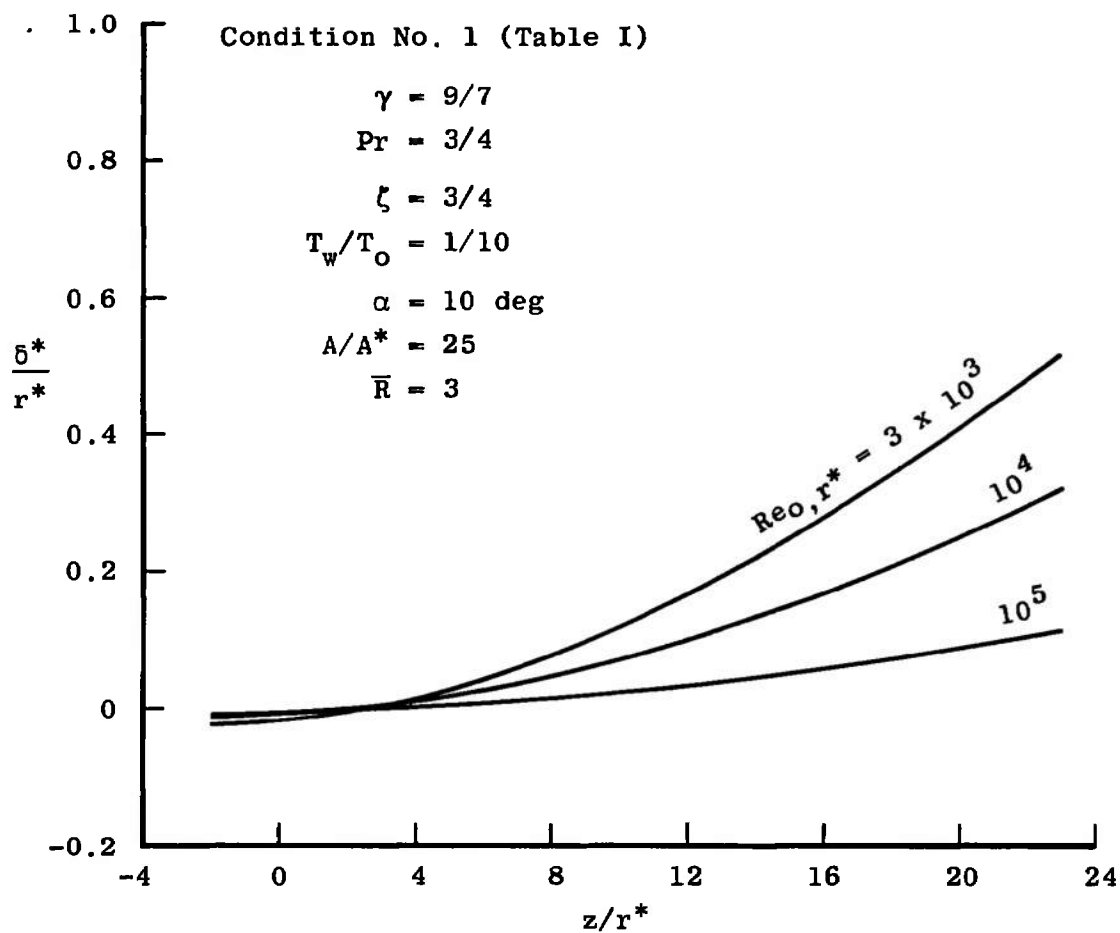


Fig. 3 Displacement Thickness for Condition No 1 (Table I)

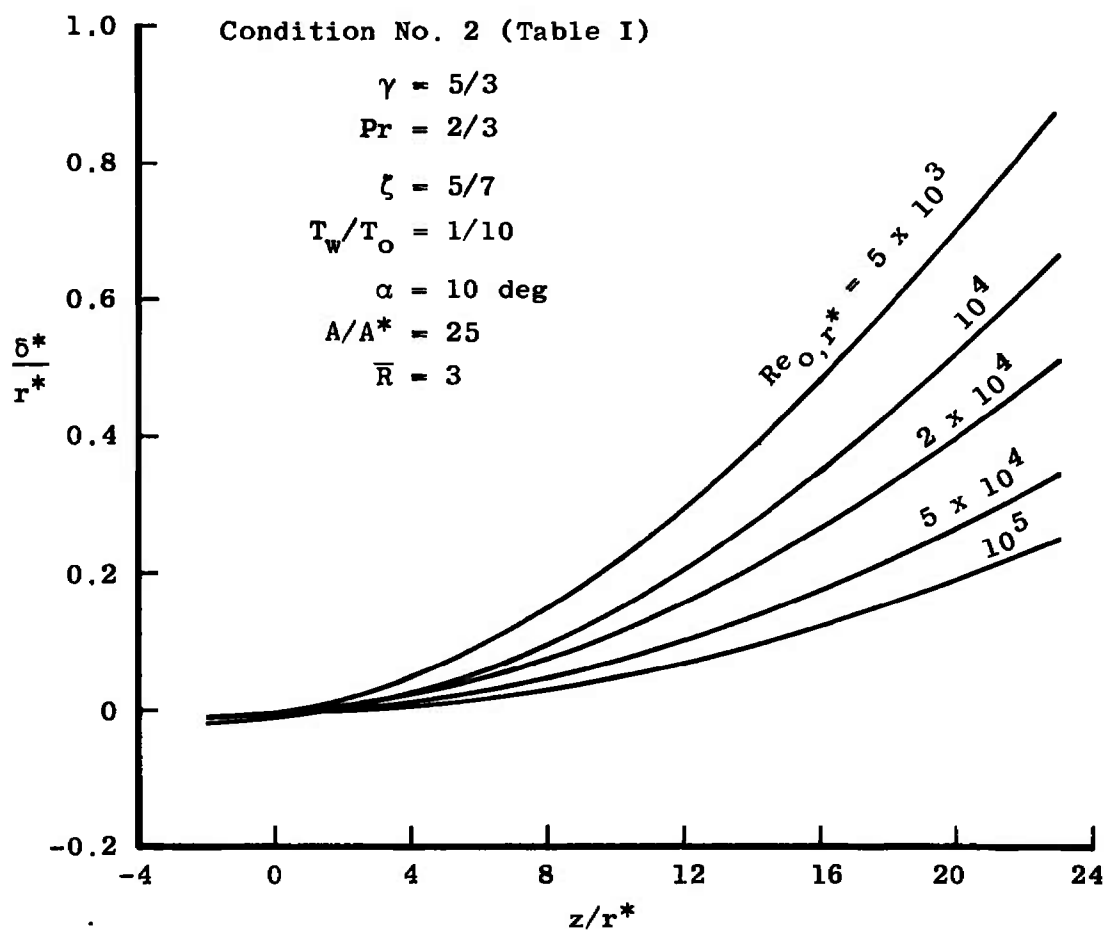


Fig. 4 Displacement Thickness for Condition No. 2 (Table I)

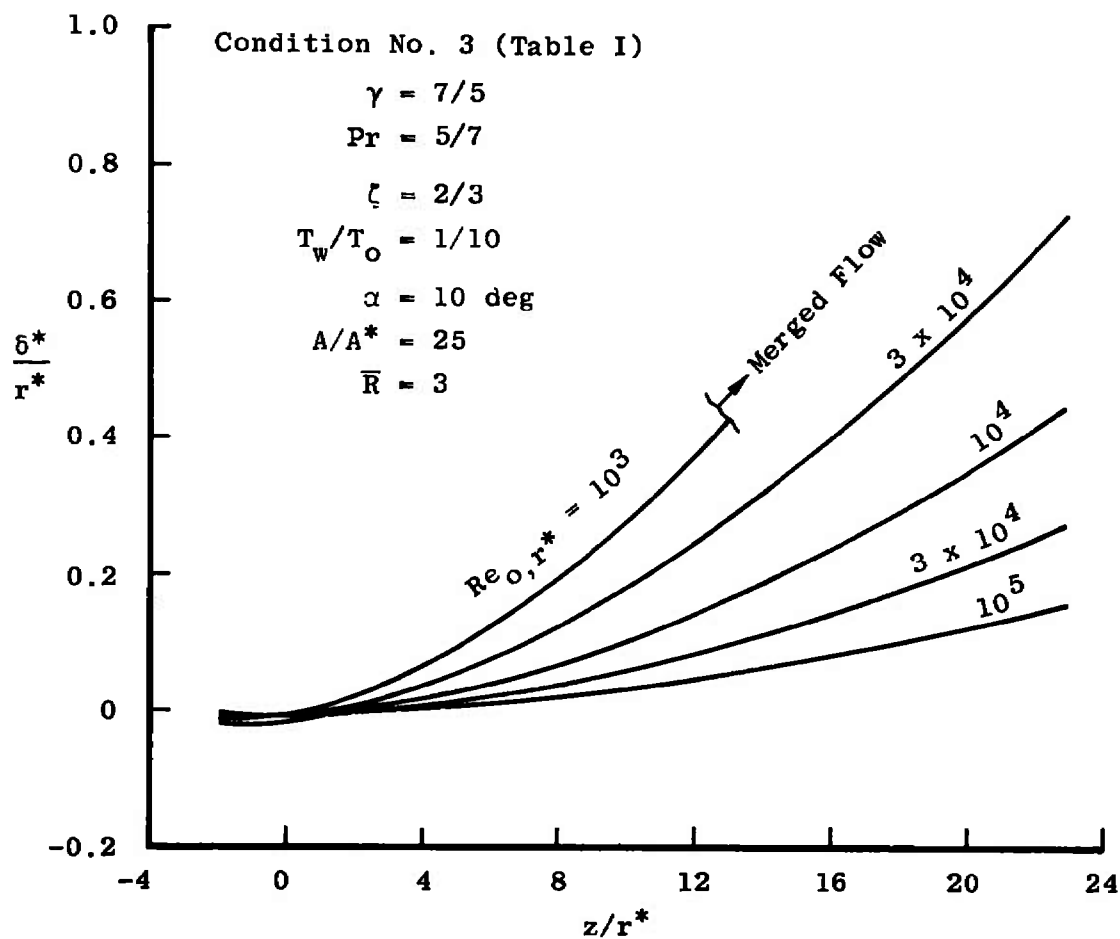


Fig. 5 Displacement Thickness for Condition No. 3 (Table I)



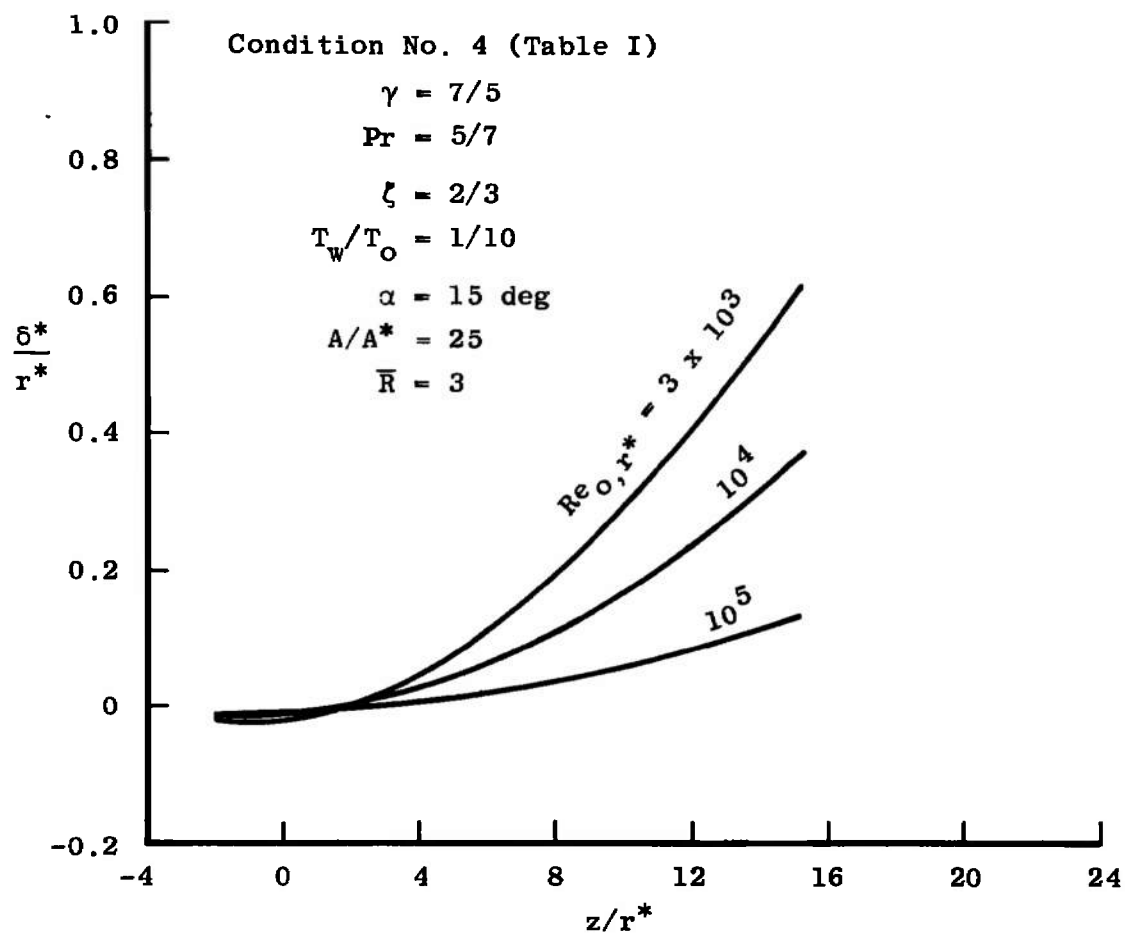


Fig. 6 Displacement Thickness for Condition No. 4 (Table I)

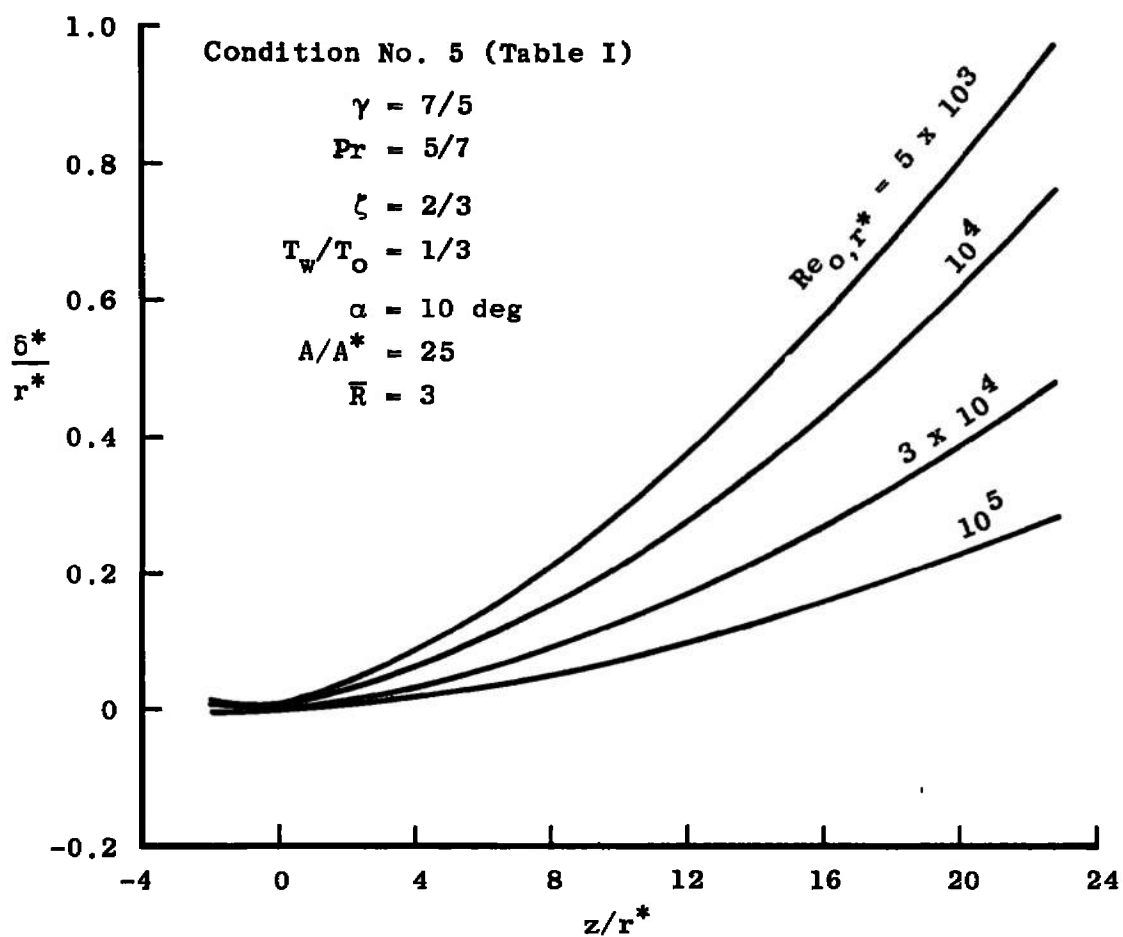


Fig. 7 Displacement Thickness for Condition No. 5 (Table I)

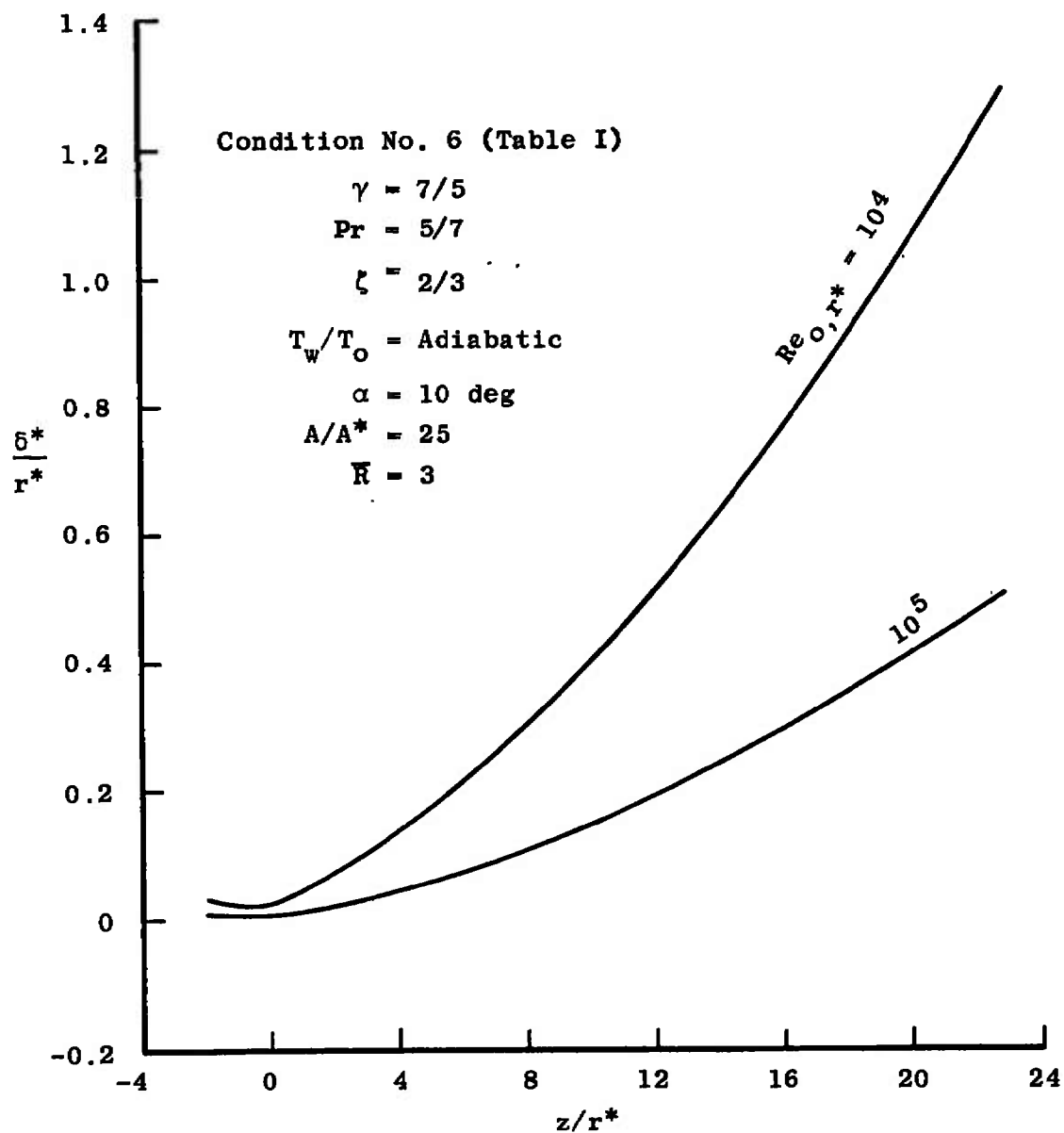


Fig. 8 Displacement Thickness for Condition No. 6 (Table I)

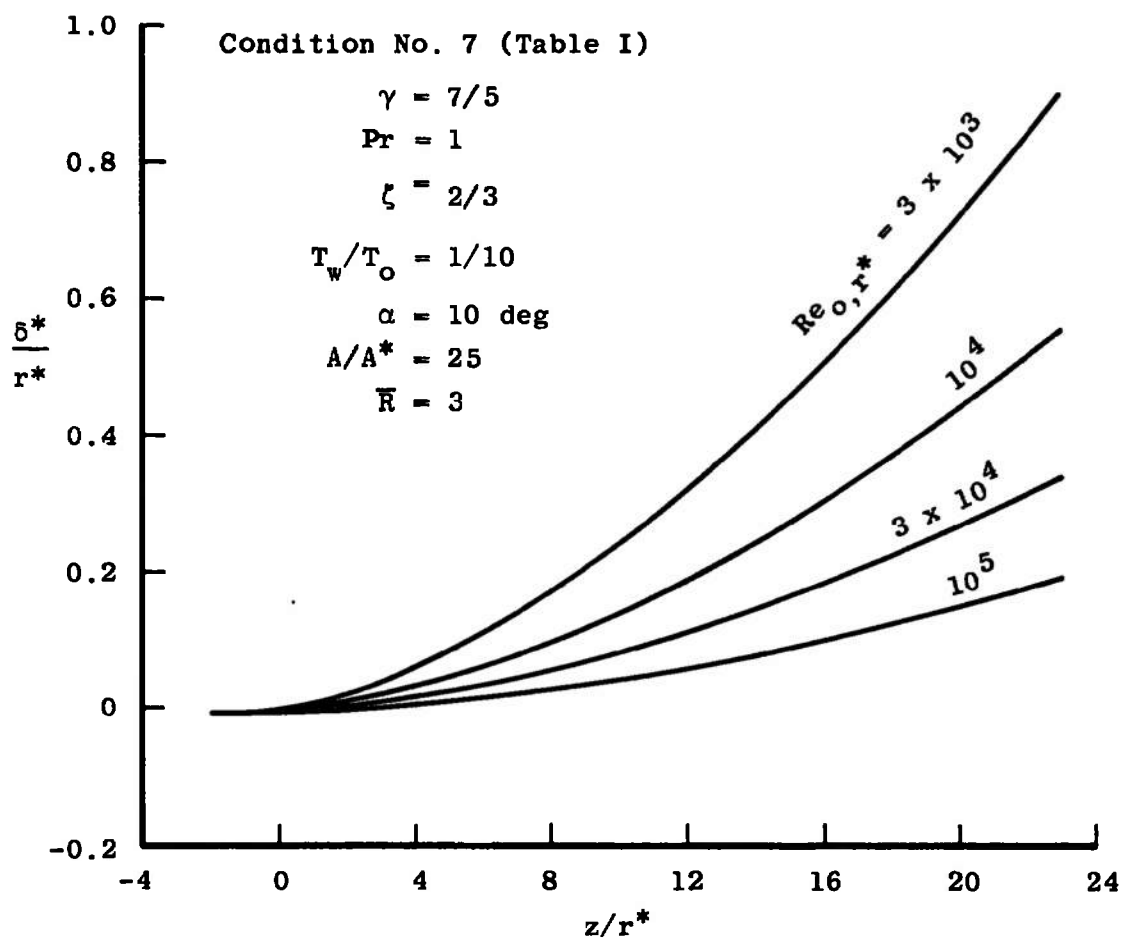


Fig. 9 Displacement Thickness for Condition No. 7 (Table I)

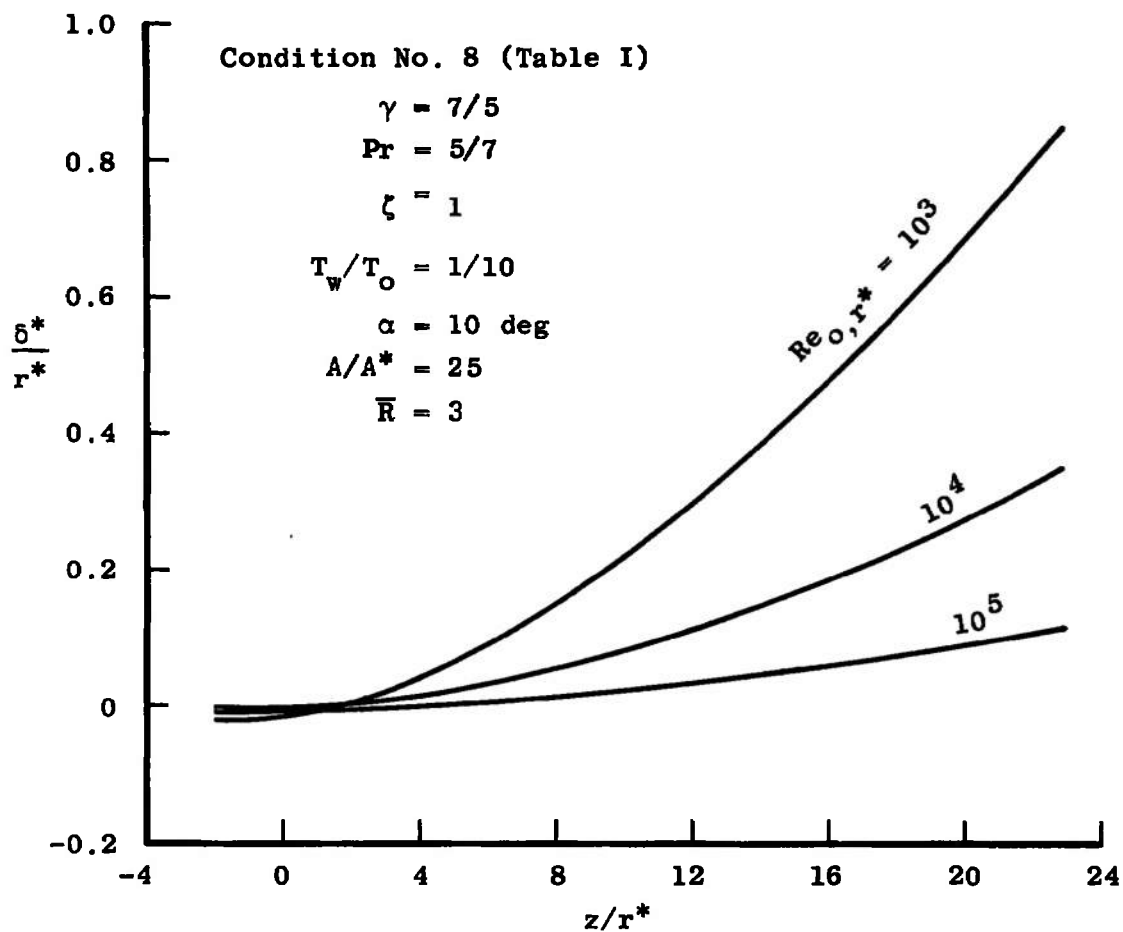


Fig. 10 Displacement Thickness for Condition No. 8 (Table I)

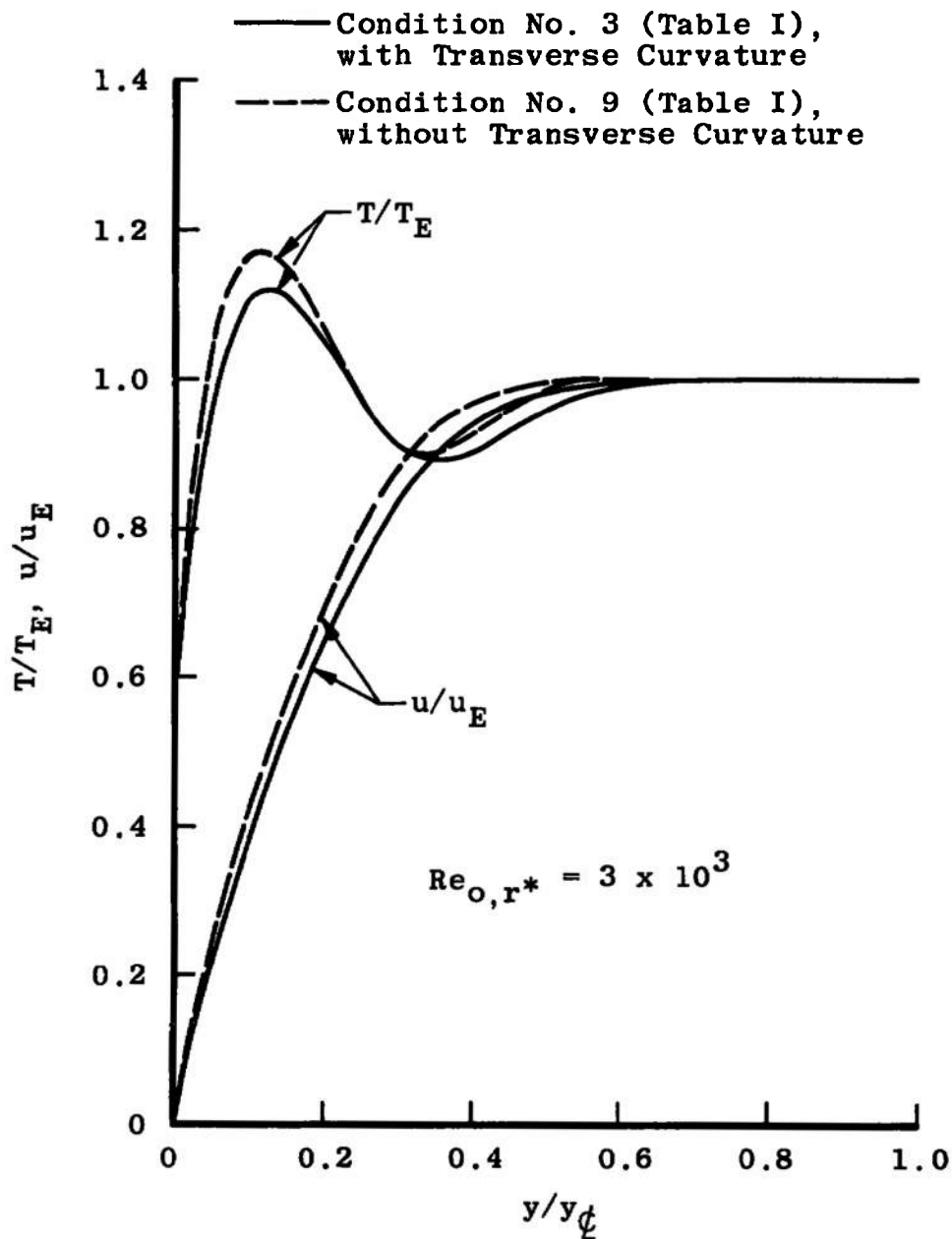


Fig. 11 Nozzle Exit Velocity and Temperature Profiles  
for Condition Nos. 3 and 9 (Table I)

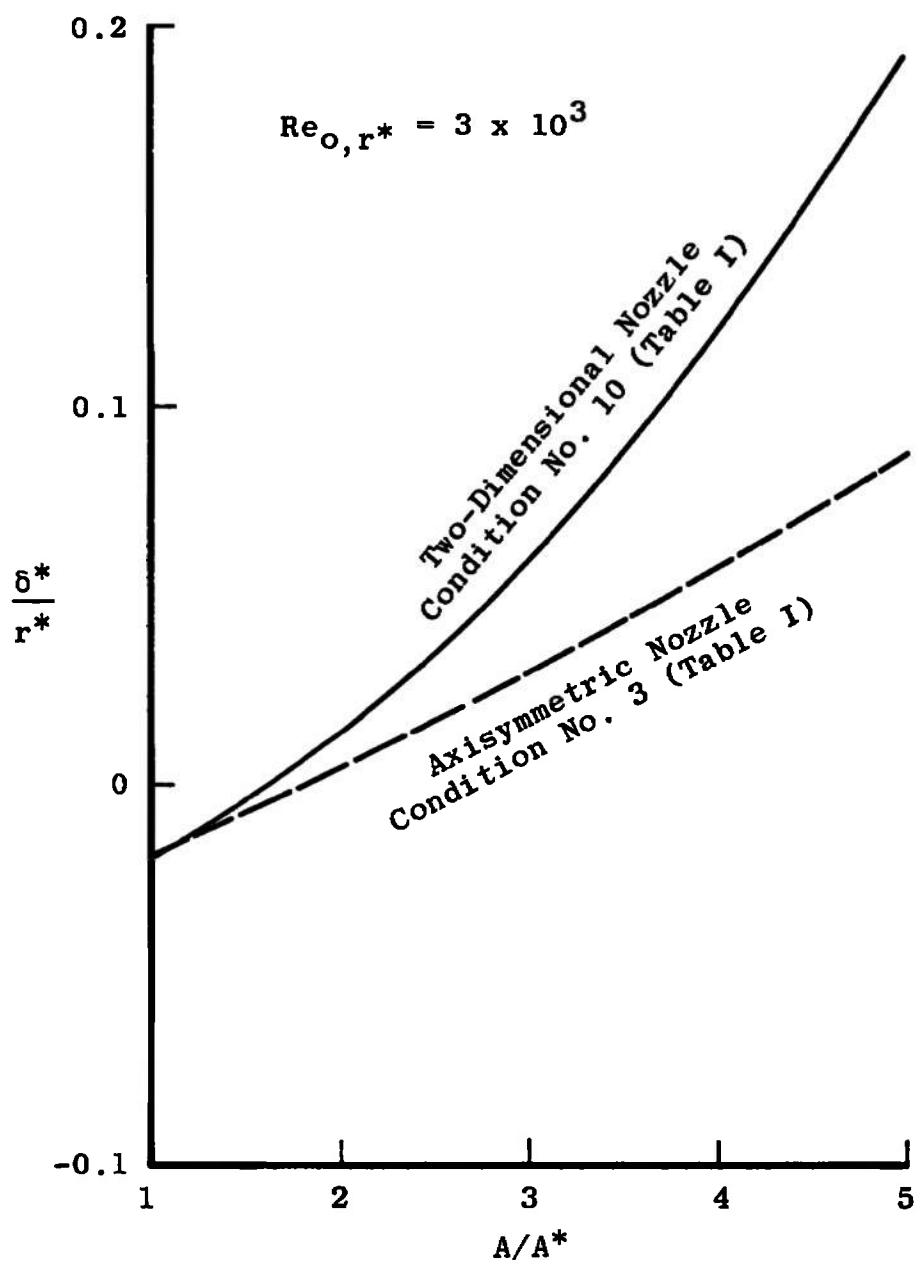


Fig. 12 Displacement Thicknesses of an Axisymmetric and Two-Dimensional Nozzle with Equal Area Ratios

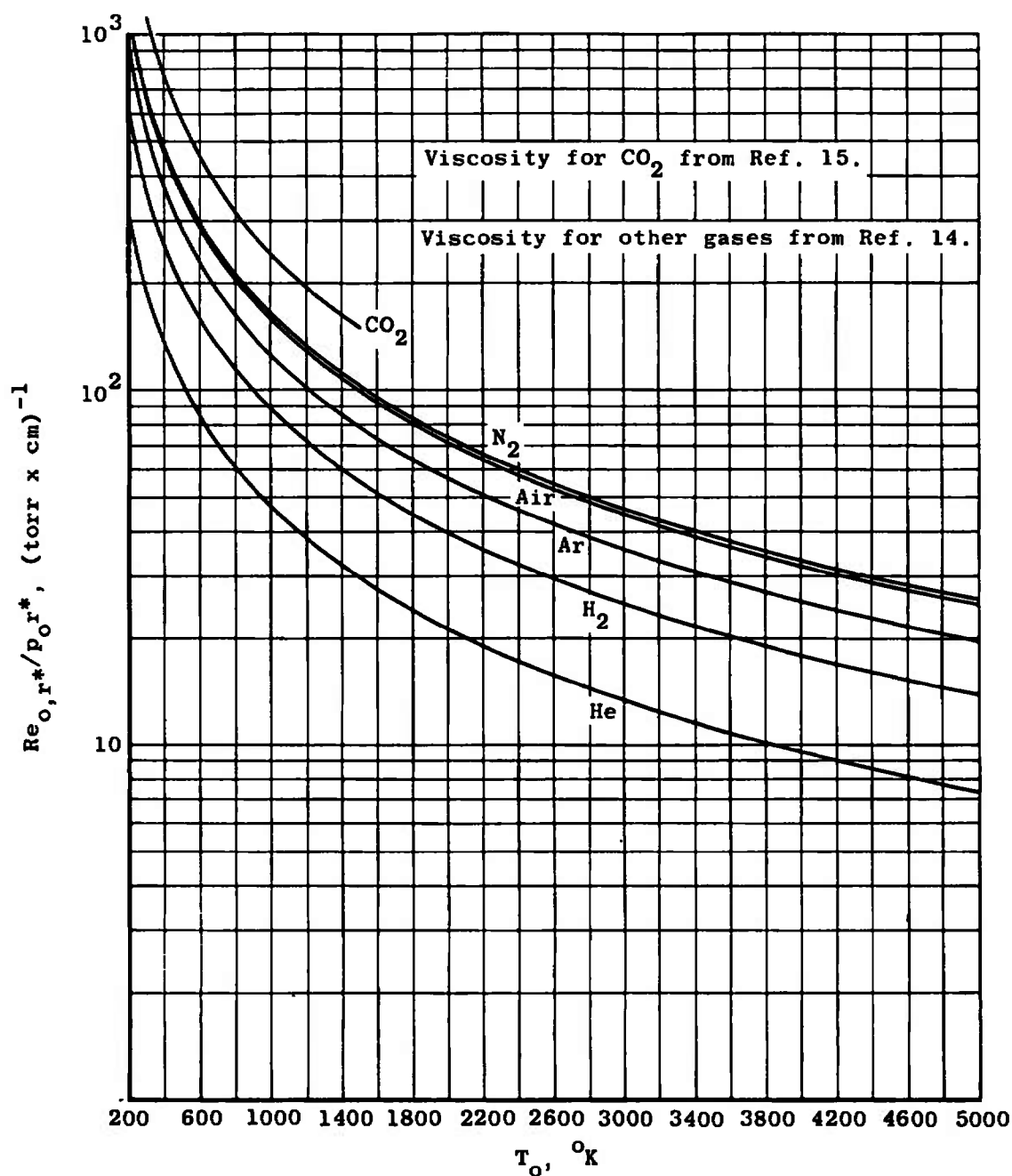


Fig. 13 Reservoir Reynolds Number as a Function of  $p_o$ ,  $T_o$ , and  $r^*$  for Various Gases



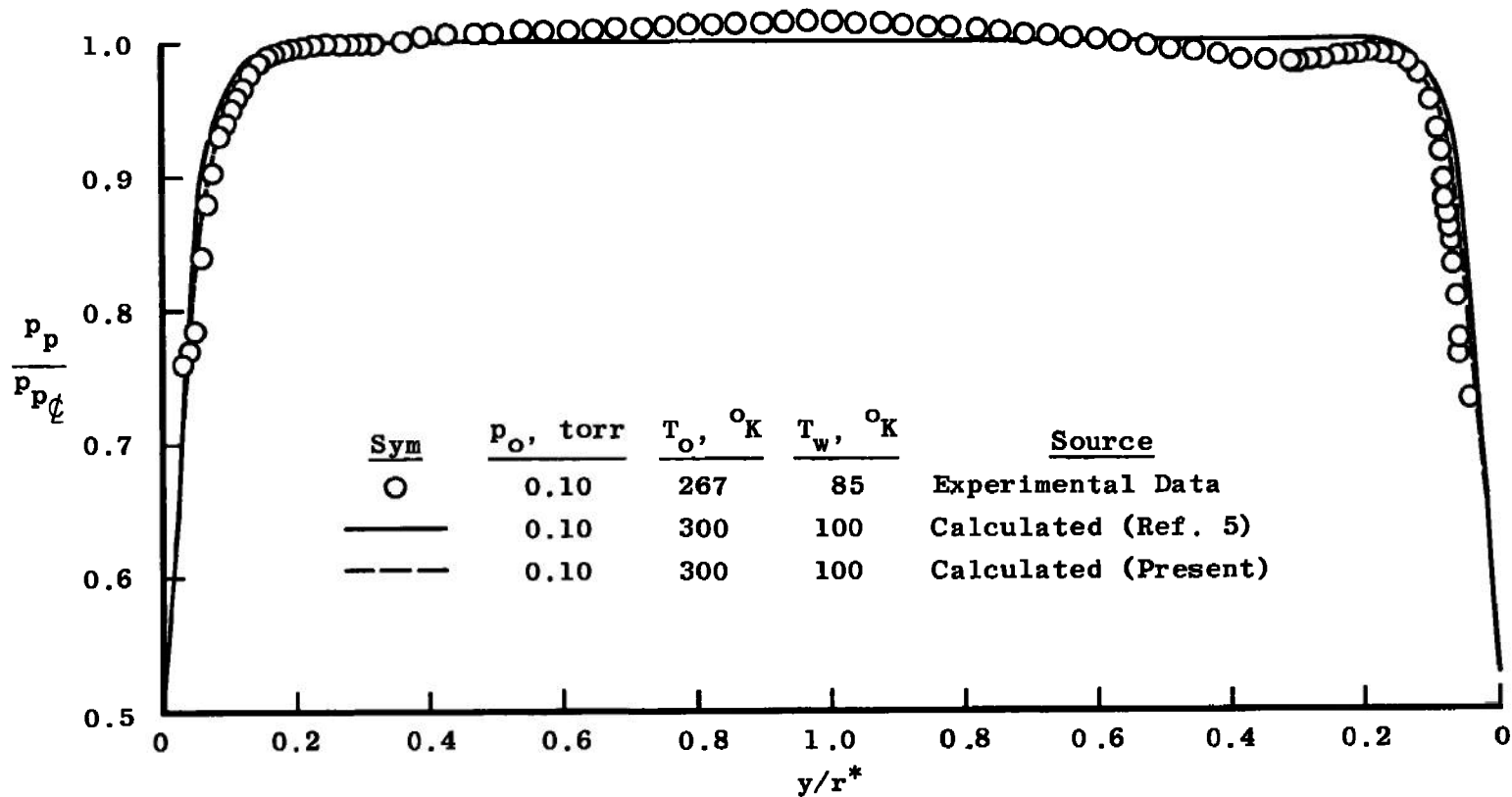


Fig. 14 Calculated and Measured Pitot Pressure Profiles at the M3 Nozzle Throat for  $Re_{o,r} = 900$

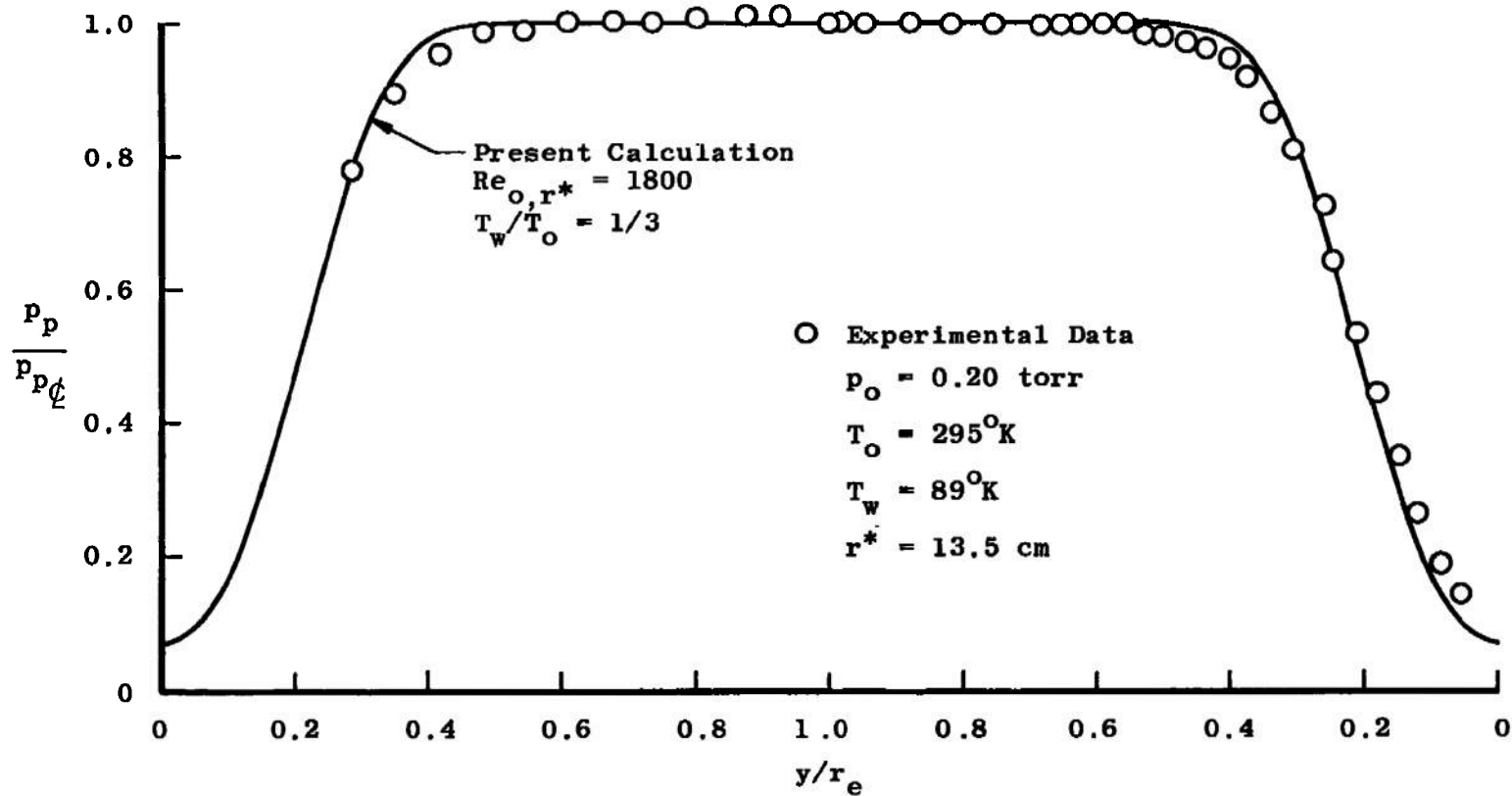


Fig. 15 Calculated and Measured Pitot Pressure Profiles  
 at the M3 Nozzle Exit for  $Re_{o,r^*} = 1800$

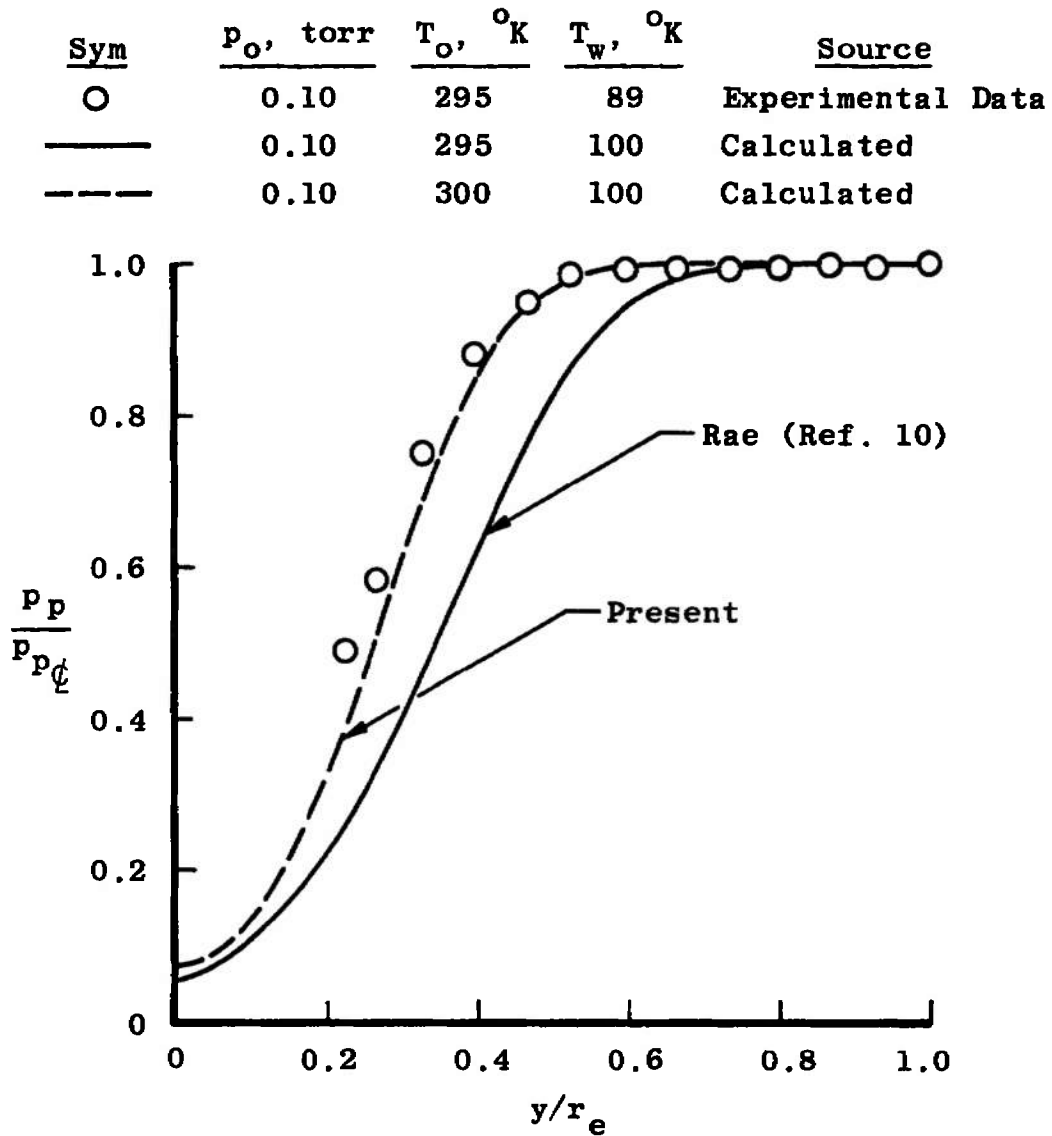
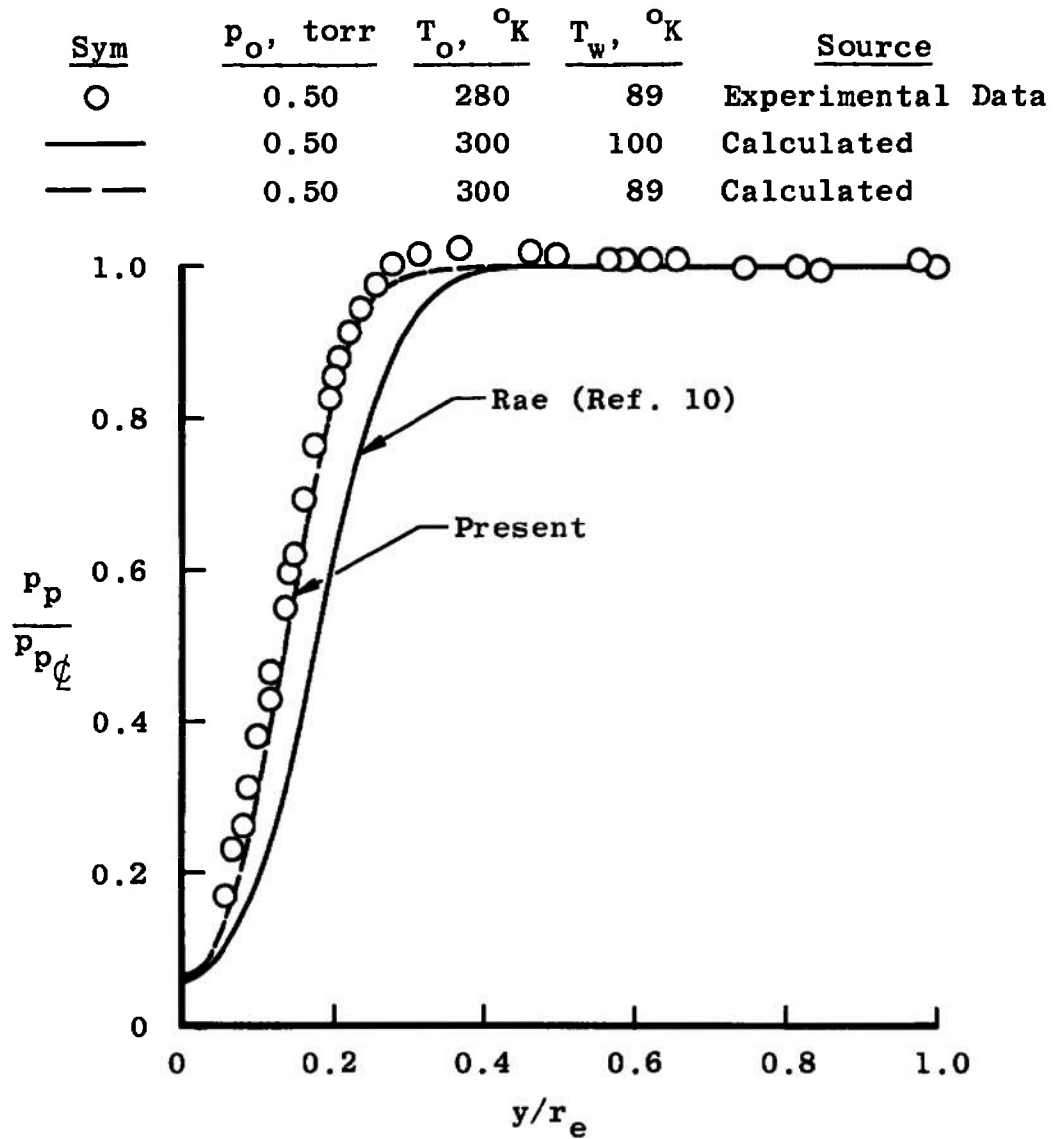


Fig. 16 Calculated and Measured Pitot Pressure Profiles  
at the M3 Nozzle Exit for  $Re_{0,r} = 900$



**Fig. 17 Calculated and Measured Pitot Pressure Profiles  
at the M3 Nozzle Exit for  $Re_{0,r} = 4500$**

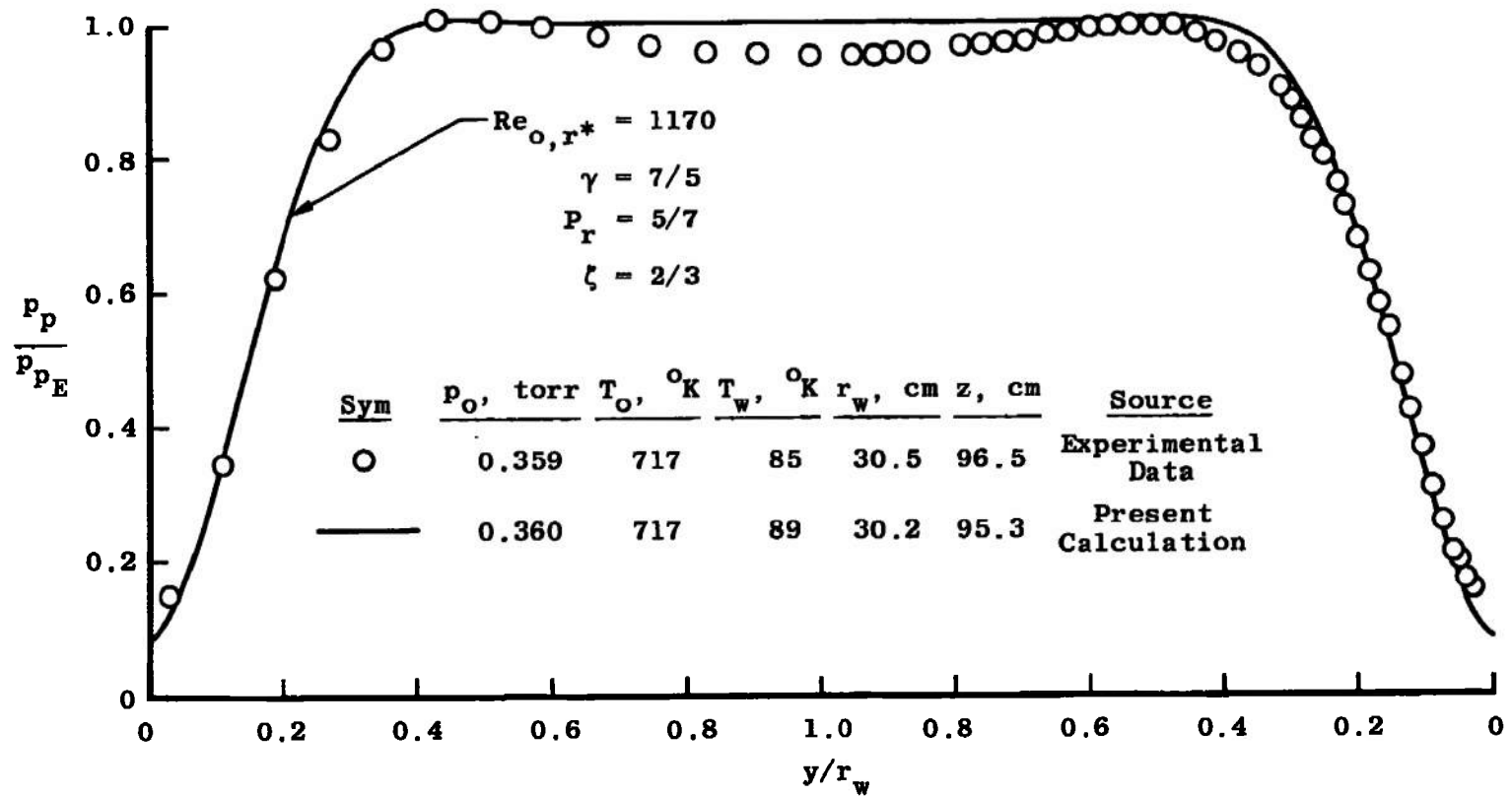


Fig. 18 Calculated and Measured Pitot Pressure Profiles Downstream of the M3 Nozzle Throat for  $Re_{o,r^*} = 1170$

<u>Sym</u>	<u>p<sub>o</sub>, torr</u>	<u>T<sub>o</sub>, °K</u>	<u>T<sub>w</sub>, °K</u>	<u>v<sub>w</sub>, cm</u>	<u>z, cm</u>	<u>Source</u>
○	0.103	717	85	30.5	96.5	Experimental Data
—	0.100	717	89	29.0	88.6	Present Calculation

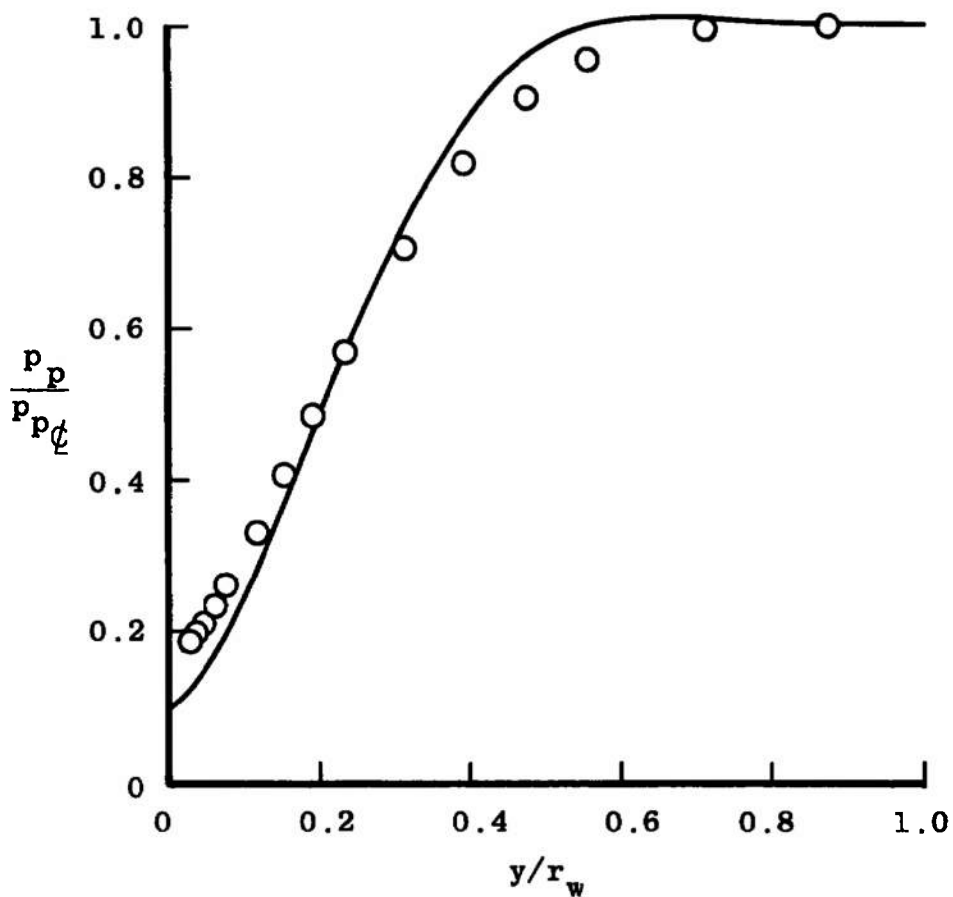


Fig. 19 Calculated and Measured Pitot Pressure Profiles Downstream of the M3 Nozzle Throat for  $Re_{o,r^*} = 330$

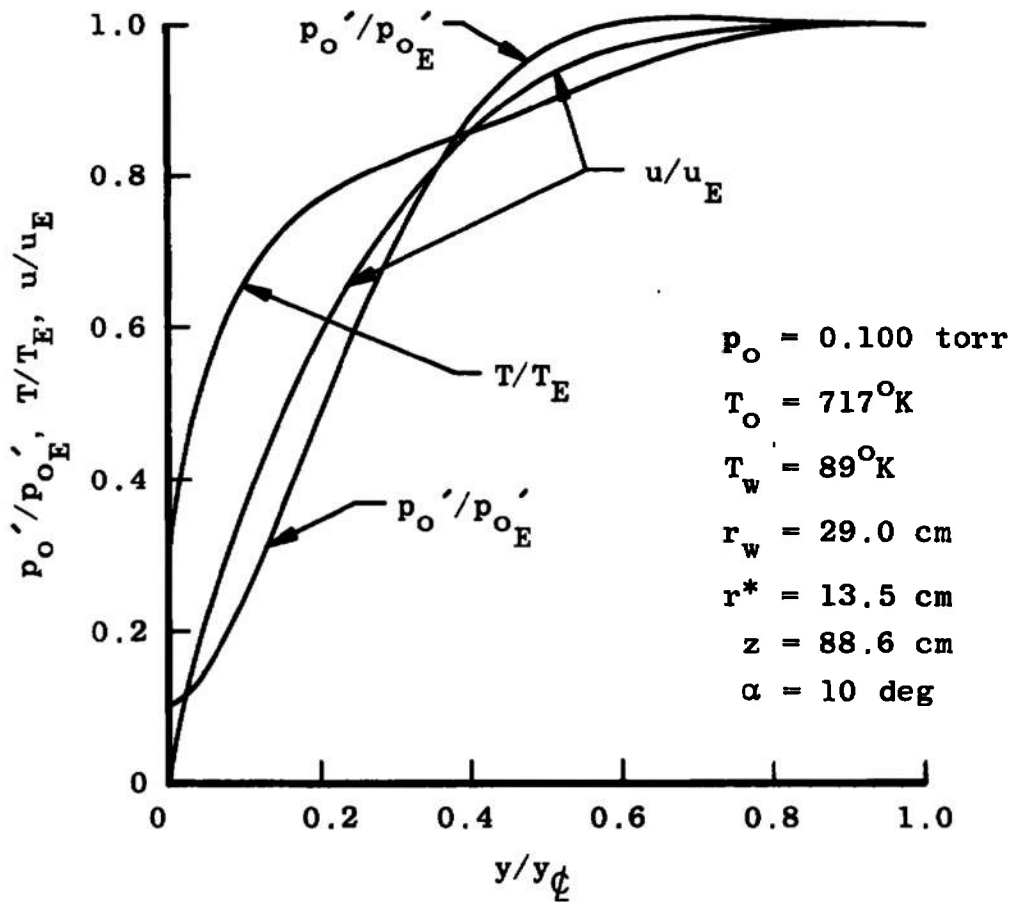


Fig. 20 Calculated Velocity, Temperature, and Pitot Pressure Profiles Downstream of the M3 Nozzle Throat for  $Re_{o,r} = 330$

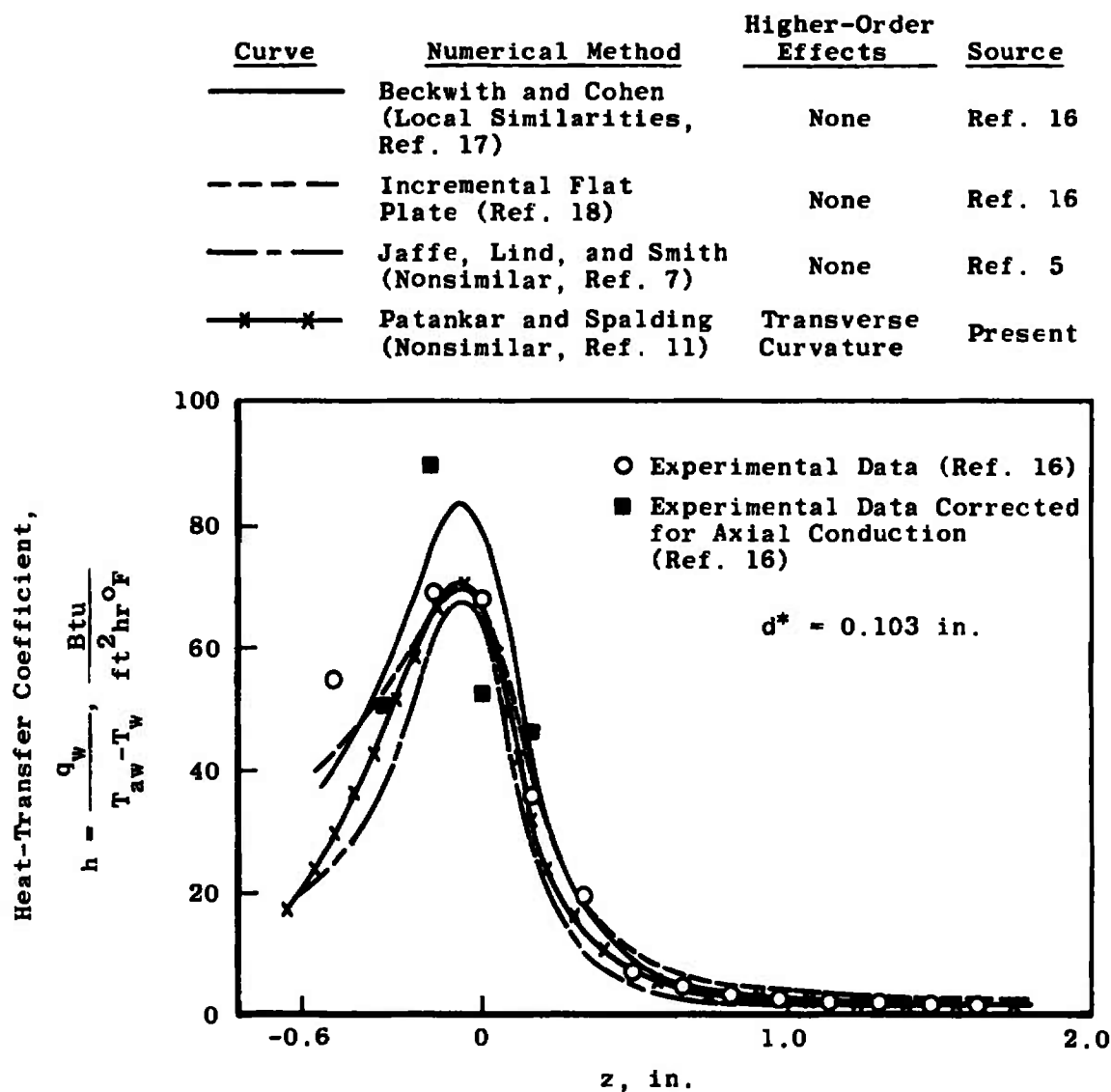


Fig. 21 Calculated and Measured Heat-Transfer Coefficients in a Low-Density Nozzle



**TABLE I**  
**CONDITIONS FOR THE NUMERICAL SOLUTIONS PRESENTED IN SECTION IV**

Condition No.	$\gamma$	Pr	$\xi$	$T_w/T_o$	$\alpha$ , deg	$A/\Lambda^*$	$\bar{R}$	$Re_{o,r^*}$	Comment
1	9/7	3/4	3/4	1/10	10	25	3	$3 \times 10^3, 10^4, 10^5$	Axisymmetric Nozzle with Transverse Curvature
2	5/3	2/3	5/7	↓	10	↓	↓	$5 \times 10^3, 10^4, 2 \times 10^4, 5 \times 10^4, 10^5$	
3	7/5	5/7	2/3	↓	10	↓	↓	$10^3, 3 \times 10^3, 10^4, 3 \times 10^4, 10^5$	
4	↓	↓	↓	↓	15	↓	↓	$3 \times 10^3, 10^4, 10^5$	
5	↓	↓	↓	1/3	10	↓	↓	$5 \times 10^3, 10^4, 3 \times 10^4, 10^5$	
6	↓	↓	↓	Adiabatic	↓	↓	↓	$10^4, 10^5$	
7	↓	1	↓	1/10	↓	↓	↓	$3 \times 10^3, 10^4, 3 \times 10^4, 10^5$	
8	↓	5/7	1	↓	↓	↓	↓	$10^3, 10^4, 10^5$	Axisymmetric Nozzle with- out Transverse Curvature
9	↓	5/7	2/3	↓	↓	↓	↓	$3 \times 10^3$	
10	↓	5/7	2/3	↓	↓	5	9	$3 \times 10^3$	Two-Dimensional Nozzle

# APPENDIX III BOUNDARY-LAYER COMPUTER CODE

FORTRAN IV G LEVEL	20	MAIN	DATE = 72286	22/52/18
	C	MAIN		A 2
0001		COMMON /GEN/ PEI,AMI,AME,OPDX,PREF(2),PR(2),P(2),DEN,AMU,XU,XD,XP,		A 3
		1XL,DX,INTG,CSALFA,ALPHA,XR,REORS,GAM,ZETA,PP0,TWTO,YSTART,USUP,IDI		A 4
		2MEN,IHEAT,Z,YD,XSTEP/1/N,NP1,NP2,NP3,NEQ,NPH,KEX,KIN,KASE,KRAO,B/B		A 5
		3ETA,GAMA(2),TAUI,TAUE,AJI(2),AJE(2),INDI(2),INDE(2)/V/U(200),F(2,2		A 6
		400),R(200),RHO(200),OM(200),Y(200)/C/SC(200),AU(200),BU(200),CU(20		A 7
		50),A(2,200),B(2,200),C(2,200)/O/YR(200),UR(200),RR(200),HR(200),XM		A 8
		6(200),PITOT(200),TEMP(200)/E/DSTAR(300),XRS(300),RWRS(300),COSAL(3		A 9
		700)		A 10
0002		COMMON /L/ AK,ALMG		A 11
0003	1	CONTINUE		A 12
0004		AK=1.		A 13
0005		INTG=0		A 14
0006		CALL BEGIN		A 15
0007		CALL PRE (XU,OPDX)		A 16
0008		XTHOAT=3.14159*XR/2.		A 17
0009		AMI=0.		A 18
0010		AME=0.		A 19
0011		GO TO 3		A 20
0012	2	CALL READY		A 21
	C	THE FOLLOWING STATEMENT IS TO KILL SHOT IF PROBLEMS (LIKE MERGING)		A 22
	C	OCCUR IN SUBROUTINE READY		A 23
0013		IF (XD.GT.XL) GO TO 13		A 24
0014	3	CONTINUE		A 25
0015		INTG=INTG+1		A 26
	C	CHOICE OF FORWARD STEP		A 27
0016		DX=XSTEP*R(1)		A 28
0017		XD=XU+DX		A 29
0018		IF (.NOT.(XU.LT.XTHOAT.AND.XD.GT.XTHOAT)) GO TO 4		A 30
0019		XD=XTHOAT		A 31
0020		DX=XD-XU		A 32
0021		ITHOAT=INTG+1		A 33
0022	4	CONTINUE		A 34
0023		IF (XD.LE.XL) GO TO 5		A 35
0024		XD=XL		A 36
0025		DX=XD-XU		A 37
0026	5	CONTINUE		A 38
0027		CALL PRE (XD,OPDX)		A 39
0028		CALL ENTRN		A 40
0029		CALL PRE (XU,OPDX)		A 41
0030		IF (KASE.EQ.2) GO TO 6		A 42
0031		IF (KIN.EQ.1) CALL MASS (XU,XD,AMI)		A 43
0032		IF (KEX.EQ.1) CALL MASS (XU,XD,AME)		A 44
0033		CALL WALL		A 45
0034	6	CALL OUTPUT		A 46
0035		CALL PRE (XD,OPDX)		A 47
0036		CALL COEFF		A 48
	C	SETTING UP VELOCITIES AT A FREE BOUNDARY		A 49
	C	MODIFIED FOLLOWING STATEMENT FOR INTERNAL CORE FLOW		A 50
0037		IF (KEX.EQ.2) U(NP3)=SQRT(2.)*SQRT(1.-PP0*((GAM-1.)/GAM))		A 51
0038		IF (KIN.EQ.2) U(1)=SQRT(U(1)*U(1)-2.*(XD-XU)*OPDX/RHO(1))		A 52
0039		CALL SOLVE (AU,BU,CU,U,NP3)		A 53
	C	SETTING UP VELOCITIES AT A SYMMETRY LINE		A 54
0040		IF (KIN.NE.3) GO TO 7		A 55
0041		U(1)=U(2)		A 56
0042		IF (KRAO.EQ.0) U(1)=.75*U(2)+.25*U(3)		A 57

FORTRAN IV G LEVEL		20	MAIN	DATE = 72286	22/52/18
0043	7		IF (KEX.EQ.3) U(NP3)=.75*U(NP2)+.25*U(NP1)	A	58
0044			IF (NEQ.EQ.1) GO TO 14	A	59
0045			DO 13 J=1,NPH	A	60
0046			DO 8 I=2,NP2	A	61
0047			AU(I)=A(J,I)	A	62
0048			BU(I)=B(J,I)	A	63
0049	8		CU(I)=C(J,I)	A	64
0050			DO 9 I=1,NP3	A	65
0051	9		SC(I)=F(J,I)	A	66
0052			CALL SOLVE (AU,BU,CU,SC,NP3)	A	67
0053			DO 10 I=1,NP3	A	68
0054	10		F(J,I)=SC(I)	A	69
0055			IF (KASE.EQ.2) GO TO 11	A	70
0056	C		SETTING UP WALL VALUES OF F	A	71
			IF (KIN.EQ.1.AND.INDI(J).EQ.2) F(J,1)=(1.+BETA+GAMA(J))*F(J,2)-(1	A	72
			1.+BETA-GAMA(J))*F(J,3))*5/GAMA(J)	A	73
0057			IF (KEX.EQ.1.AND.INDE(J).EQ.2) F(J,NP3)=(1.+BETA+GAMA(J))*F(J,NP2	A	74
			1)-(1.+BETA-GAMA(J))*F(J,NP1))*5/GAMA(J)	A	75
	C		SETTING UP SYMMETRY-LINE VALUES OF F	A	76
0058	11		IF (KIN.NE.3) GO TO 12	A	77
0059			F(J,1)=F(J,2)	A	78
0060			IF (KRAO.EQ.0) F(J,1)=.75*F(J,2)+.25*F(J,3)	A	79
0061	12		IF (KEX.EQ.3) F(J,NP3)=.75*F(J,NP2)+.25*F(J,NP1)	A	80
0062	13		CONTINUE	A	81
0063	14		XP=XU	A	82
0064			XRS(INTG)=XU	A	83
0065			RWPS(INTG)=R(1)	A	84
0066			COSAL(INTG)=CSALFA	A	85
0067			XU=XD	A	86
0068			PEI=PEI+DX*(R(1)*AMI-R(NP3)*AME)	A	87
	C		THE TERMINATION CONDITION	A	88
0069	1		IF (XU.LT.XL) GO TO 2	A	89
0070			CALL NEWPPD	A	90
0071			STOP	A	91
0072			END	A	92-

FORTRAN IV G LEVEL 20		NEWPPO	DATE = 72286	22/52/18	
0001		SUBROUTINE NEWPPO		B	1
0002		COMMON /GEN/ PEI,AMI,AME,OPDA,PREFI21,PR(21,P12),DEN,AMU,XU,XD,XP,		B	2
		IXL,DX,INTG,CSALFA,ALPHA,XR,REORS,GAM,ZETA,PPO,TWTU,YSTART,USUP,IDI		B	3
		ZMEN,IHEAT,Z,TU,XSTEP/E/DSTAR(300),XRS(300),RWRS(300),COSAL(300)		B	4
0003		DIMENSION FMM(300),POP(300),RIRS(300)		B	5
0004		IF (IDIMEN.EQ.0) RETURN		B	6
0005		G=GAM		B	7
0006		C1=IG+1./2.		B	8
0007		C2=IG-1./2.		B	9
0008		C3=IG+1./12.*IG-1.)		B	10
0009		C4=C1**C3		B	11
0010		C5=C4*C2*C3*2.		B	12
0011		DO 1 I=1,INTG		B	13
0012	1	RIPS(I)=RWRS(I)-COSAL(I)*DSTAR(I)		B	14
0013		DO 2 I=1,INTG		B	15
0014		IF (RIRS(I).LT.RIRS(I+1)) GO TO 3		B	16
0015	2	CONTINUE		B	17
0016	3	RTHOAT=RWRS(I)-COSAL(I)*DSTAR(I)		B	18
0017		DO 14 I=1,INTG		B	19
0018		A=(RTHOAT/RIRS(I))**2		B	20
0019		IF (I-1) 4,4,6		B	21
0020	4	FM1=0.5		B	22
0021	5	B=(1.+C2*FM1**2)		B	23
0022		FM=FM1-(A*B**((C3+1.-C4*FM1*B)/C5*FM1**2-C4*B)		B	24
0023		IF (ABS(FM-FM1)-.00001) 13,12,12		B	25
0024	6	IF (A-1.0) 8,7,7		B	26
0025	7	FM=1.0		B	27
0026		B=(1.+C2)		B	28
0027		GO TO 13		B	29
0028	8	CONTINUE		B	30
0029		IF (FM-1.0) 9,10,10		B	31
0030	9	FM1=FM		B	32
0031		GO TO 11		B	33
0032	10	FM1=FM*0.1		B	34
0033	11	CONTINUE		B	35
0034		GO TO 5		B	36
0035	12	FM1=FM		B	37
0036		GO TO 5		B	38
0037	13	POP(I)=B**IG/(1.-G)		B	39
0038		FMM(I)=FM		B	40
0039	14	CONTINUE		B	41
0040		WRITE (6,15)		B	42
0041		WRITE (7,16) INTG		B	43
0042		WRITE (7,17) (XRS(I),POP(I),I,I=1,INTG)		B	44
0043		WRITE (6,18) (FMM(I),POP(I),DSTAR(I),XRS(I),RWRS(I),I,I=1,INTG)		B	45
0044		RETURN		B	46
	C			B	47
0045	15	FORMAT(11H1,2X,'THE DISPLACEMENT THICKNESS FROM THIS ITERATION AND		B	48
		1THE PRESSURE DISTRIBUTION FOR THE NEXT ITERATION FOLLOWS'//,		B	49
		28X,'M',11X,'P/PO',11X,'DS',13X,'X',12X,'RW',8X,'INTG'//)		B	50
0046	16	FORMAT(13)		B	51
0047	17	FORMAT(1P2E12,6,53X,13)		B	52
0048	18	FORMAT(1P5E14,5,16)		B	53
0049		END		B	54

FORTRAN IV G LEVEL 20		BEGIN	DATE = 72286	22/52/18
0001		SUBROUTINE BEGIN		C 1
0002		COMMON /GEN/ PEI,AMI,AME,DPOX,PREF(2),PR(2),P(2),DEN,AMU,XU,XD,XP,		C 2
		1XL,OX,INTG,CSALFA,ALPHA,XR,REORS,GAM,ZETA,PPD,TWTO,YSTART,USUP,IOI		C 3
		2MEN,IHEAT,Z,TU,XSTEP/1/N,NP1,NP2,NP3,NEQ,NPH,KEX,KIN,KASE,KRAO/B/B		C 4
		3ETA,GAMA(2),TAUI,TAUE,AJI(2),AJE(2),INDI(2),INDE(2)/V/U(200),F(2,2		C 5
		400),R(200),RHO(200),OM(200),Y(200)		C 6
	C	PROBLEM SPECIFICATION		C 7
0003		READ (5,28) KRAD,IDIMEN,NEQ,KEX,KIN,IHEAT,N		C 8
0004		READ (5,29) REORS,ZETA,PR(1),GAM,ALPHA,XR,XL,USUP,YSTART,TWTO,XSTE		C 9
		1P		C 10
	C	IDIMEN=0 FOR PLANAR FLOW AND IDIMEN=1 FOR AXISYMMETRIC FLOW		C 11
	C	INITIAL EDGE OF BOUNDARY LAYER IS YSTART		C 12
0005		PREF(1)=PR(1)		C 13
	C	APPROXIMATE CALCULATION OF UEDGE FROM ONE DIMENSION FLOW RELATIONS		C 14
0006		UUMXX=SQRT(2./((GAM-1.)*(GAM+1./2.)*((GAM+1.)/(2.*(GAM-1.)))		C 15
0007		UUMXX=(1./(1.+XR))*((1+IDIMEN)/UUMXX		C 16
0008		UEdge=UUMXX*SQRT(2.)		C 17
0009		KASE=2		C 18
0010		IF (KIN.EQ.1.OR.KEX.EQ.1) KASE=1		C 19
0011		XU=0.		C 20
0012		NPH=NEQ-1		C 21
0013		NP1=N+1		C 22
0014		NP2=N+2		C 23
0015		NP3=N+3		C 24
	C	INITIAL VELOCITY PROFILE		C 25
0016		Y(1)=0.0		C 26
0017		U(1)=0.0		C 27
0018		XNP2=NP2		C 28
0019		DELY=YSTART/XNP2		C 29
0020		DO 1 I=2,NP3		C 30
0021		Y(I)=Y(I-1)+DELY		C 31
0022		ETA=Y(I)/(DELY*XNP2)		C 32
0023		U(I)=(2.*ETA-ETA**2)*UEdge		C 33
0024	1	CONTINUE		C 34
	C	CALCULATION OF SLIP VELOCITIES AND DISTANCES		C 35
0025		BETA=1.0		C 36
0026		GO TO (2,3,4), KIN		C 37
0027	2	U(2)=U(3)/(1.+2.*BETA)		C 38
0028		Y(2)=Y(3)*BETA/(2.+BETA)		C 39
0029		GO TO 6		C 40
0030	3	U11=U(1)*U(1)		C 41
0031		U13=U(1)*U(3)		C 42
0032		U33=U(3)*U(3)		C 43
0033		SQ=8.*U11-12.*U13+9.*U33		C 44
0034		U(2)=(16.*U11-4.*U13+U33)/(2.*(U(1)+U(3))+SQRY(SQ))		C 45
0035		Y(2)=Y(3)*(U(2)+U(3)-2.*U(1))*5/(U(2)+U(3)+U(1))		C 46
0036		GO TO 6		C 47
0037	4	IF (KRAD.NE.0) GO TO 5		C 48
0038		U(2)=(4.*U(1)-U(3))/3.		C 49
0039		Y(2)=0.		C 50
0040		GO TO 6		C 51
0041	5	U(2)=U(1)		C 52
0042		Y(2)=Y(3)/3.		C 53
0043	6	GO TO (7,8,9), KEX		C 54
0044	7	U(NP2)=U(NP1)/(1.+2.*BETA)		C 55
0045		Y(NP2)=Y(NP3)-(Y(NP3)-Y(NP1))*BETA/(2.+BETA)		C 56

FORTRAN IV G LEVEL 20		BEGIN	DATE = 72286	22/52/18	
0046		GO TO 10		C	57
0047	B	U11=U(NP1)*U(NP1)		C	58
0048		U13=U(NP1)*U(NP3)		C	59
0049		U33=U(NP3)*U(NP3)		C	60
0050	.	SQ=44.*U33-12.*U13+9.*U11		C	61
0051		U(NP2)=(16.*U33-4.*U13+U11)/(2.*(U(NP1)+U(NP3))+SQRT(SQ))		C	62
0052		Y(NP2)=Y(NP3)-(Y(NP3)-Y(NP1))*(U(NP2)+U(NP1)-2.*U(NP3))*5/(U(NP2)+U(NP1)+U(NP3))		C	63
0053		GO TO 10		C	65
0054	9	U(NP2)=(4.*U(NP3)-U(NP1))/3.		C	66
0055		Y(NP2)=Y(NP3)		C	67
0056	10	CONTINUE		C	68
0057		IF (NEQ.EQ.1) GO TO 20		C	69
0058		DO 19 J=1,NPH		C	70
	C	INITIAL PROFILES OF OTHER DEPENDENT VARIABLES		C	71
0059		DO 11 I=1,NP3		C	72
0060		ETA=Y(I)/(DEL V*XNP2)		C	73
0061		F(J,1)=TWTO+(2.*ETA-ETA**2)*(1.-TWTO)		C	74
0062	11	CONTINUE		C	75
	C	CALCULATION OF CORRESPONDING SLIP VALUES		C	76
0063		GAMA(J)=1.0		C	77
0064		GO TO (12,13,14), KIN		C	78
0065	12	F(J,2)=F(J,1)/(F(J,3)-F(J,1))*(1.+BETA-GAMA(J))/(1.+BETA+GAMA(J))		C	79
0066		GO TO 15		C	80
0067	13	G=(U(2)+U(3)-8.*U(1))/(5.*(U(2)+U(3))+8.*U(1))		C	81
0068		GF=(1.-PREF(J))/(1.+PREF(J))		C	82
0069		GF=(G+GF)/(1.+G*GF)		C	83
0070		F(J,2)=F(J,3)*GF+(1.-GF)*F(J,1)		C	84
0071		GO TO 15		C	85
0072	14	F(J,2)=F(J,1)		C	86
0073		IF (KRAD.EQ.0) F(J,2)=(4.*F(J,1)-F(J,3))/3.		C	87
0074	15	GO TO (16,17,18), KEX		C	88
0075	16	F(J,NP2)=F(J,NP3)+(F(J,NP1)-F(J,NP3))*(1.+BETA-GAMA(J))/(1.+BETA+GAMA(J))		C	89
		GAMA(J)		C	90
0076		GO TO 19		C	91
0077	17	G=(U(NP2)+U(NP1)-8.*U(NP3))/(5.*(U(NP2)+U(NP1))+8.*U(NP3))		C	92
0078		GF=(1.-PREF(J))/(1.+PREF(J))		C	93
0079		GF=(G+GF)/(1.+G*GF)		C	94
0080		F(J,NP2)=F(J,NP1)*GF+(1.-GF)*F(J,NP3)		C	95
0081		GO TO 19		C	96
0082	18	F(J,NP2)=(4.*F(J,NP3)-F(J,NP1))/3.		C	97
0083	19	CONTINUE		C	98
0084	20	CONTINUE		C	99
0085		CALL DENSTY		C	100
	C	CALCULATION OF RADI		C	101
0086		CALL RAD (XU,R(1),CSALFA)		C	102
0087		IF (CSALFA.EQ.0..OR.KRAD.EQ.0) GO TO 22		C	103
0088		DO 21 I=2,NP3		C	104
0089	21	R(I)=R(1)-Y(I)*CSALFA		C	105
	C	CHANGE MADE IN STATEMENT NUMBER 28 FOR INTERNAL FLOW		C	106
0090		GO TO 24		C	107
0091	22	DO 23 I=2,NP3		C	108
0092	23	R(I)=R(1)		C	109
0093	24	CONTINUE		C	110
	C	CALCULATION OF OMEGA VALUES		C	111
0094		OM(1)=0.		C	112

FORTRAN	IV	G	LEVEL	20	BEGIN	DATE = 72286	22/52/18
0095					OM(2)=0.		C 113
0096					DO 25 I=3,NP2		C 114
0097		25			OM(I)=OM(I-1)+.5*(RHO(I)*U(I)*R(I)+RHO(I-1)*U(I-1)*R(I-1))*(Y(I)-Y		C 115
					1(I-1))		C 116
0098					PE(=OM(NP2)		C 117
0099					DO 26 I=3,NP1		C 118
0100		26			OM(I)=OM(I)/PEI		C 119
0101					OM(NP2)=1.		C 120
0102					OM(NP3)=1.		C 121
0103					IF (NEQ.EQ.1) RETURN		C 122
0104					DO 27 J=1,NPH		C 123
0105					IF (KEX.EQ.1) INDE(J)=1		C 124
0106					IF (KIN.EQ.1) INDI(J)=1		C 125
0107		27			CONTINUE		C 126
0108					RETURN		C 127
		C					C 128
0109		28			FORMAT(6I1,I3)		C 129
0110		29			FORMAT (8E10,0)		C 130
0111					END		C 131-

FORTRAN IV G LEVEL	20	COEFF	DATE = 7-28-66	22/52/18
0001		SUBROUTINE CNEFF		0 1
0002		COMMON /GEN/ PEI,AMI,AME,DPDX,PREF(2),PR(2),P(2),DEN,AMU,XU,XD,XP,		0 2
		1XL,OX,INTG,CSALFA,ALPHA,XP,REURS,GAM,ZETA,PPD,TWTO,YSTART,USUP,IDI		0 3
		2MEN,1HEAT,Z,TD,XSTEP/1/N,NP1,NP2,NP3,NEQ,NPH,KEX,KIN,KASE,KRAD/B/B		0 4
		3ETA,GAMA(2),TAUI,TAUF,AJI(2),AJE(2),INDI(2),INDE(2)/V/U(200),F(2,2		0 5
		4OU),R(200),RHO(200),OM(200),Y(200)/C/SC(200),AU(200),BU(200),CU(20		0 6
		50),A(2,200),B(2,200),C(2,200)		0 7
0003		COMMON /L/ AK,ALMG		0 8
0004		DIMENSION G1(200), G2(200), G3(200), D1(2,200), S1(200), S2(200), S		0 9
		13(200)		0 10
	C	CALCULATION OF SMALL C 'S		0 11
0005		DO 1 I=2,NP1		0 12
0006		RA=.5*(R(I+1)+R(I))		0 13
0007		RH=.5*(RHO(I+1)+RHO(I))		0 14
0008		UH=.5*(U(I+1)+U(I))		0 15
0009		CALL VEFF (I,I+1,FMU)		0 16
0010	1	SC(I)=RA*KA*RH*UH*EMU/(PEI*PEI)		0 17
	C	THE CONVECTION TERM		0 18
0011		SA=P(1)*AMI/PEI		0 19
0012		SB=(R(NP3)*AME-R(1)*AMI)/PEI		0 20
0013		DX=XD-XU		0 21
0014		DO 4 I=3,NP1		0 22
0015		OMD=UM(I+1)-OM(I-1)		0 23
0016		P2=.25/OM		0 24
0017		P3=P2/OMD		0 25
0018		P1=(OM(I+1)-OM(I))*P3		0 26
0019		P3=(OM(I)-OM(I-1))*P3		0 27
0020		P2=.3.*P2		0 28
0021		Q=SA/OMD		0 29
0022		R2=-SB*.25		0 30
0023		R3=P2/OMD		0 31
0024		R1=-(OM(I+1)+3.*OM(I))*R3		0 32
0025		R3=(OM(I-1)+3.*OM(I))*R3		0 33
0026		G1(I)=P1+Q*R1		0 34
0027		G2(I)=P2+R2		0 35
0028		G3(I)=P3-Q*R3		0 36
0029		CU(I)=-P1*U(I+1)-P2*U(I)-P3*U(I-1)		0 37
	C	THE DIFFUSION TERM		0 38
0030		AU(I)=2./OMD		0 39
0031		BU(I)=SC(I-1)*AU(I)/(OM(I)-OM(I-1))		0 40
0032		AU(I)=SC(I)*AU(I)/(OM(I+1)-OM(I))		0 41
0033		IF (NEQ.EQ.1) GO TO 3		0 42
0034		DO 2 J=1,NPH		0 43
0035		C(J,I)=-P1*F(J,I+1)-P2*F(J,I)-P3*F(J,I-1)		0 44
0036		CALL SOURCE (J,I,CS,D(J,I))		0 45
0037		C(J,I)=-C(J,I)+CS-F(J,I)*D(J,I)		0 46
0038		A(J,I)=AU(I)/PREF(J)		0 47
0039		B(J,I)=BU(I)/PREF(J)		0 48
0040	2	CONTINUE		0 49
	C	SOURCE TERM FOR VELOCITY EQUATION		0 50
0041	3	S1(I)=DPDX*DX		0 51
0042		S2(I)=P2*S1(I)/(RHO(I)*U(I))		0 52
0043		S3(I)=P3*S1(I)/(RHO(I-1)*U(I-1))		0 53
0044		S1(I)=P1*S1(I)/(RHO(I+1)*U(I+1))		0 54
0045		CU(I)=-CU(I)-2.*(S1(I)+S2(I)+S3(I))		0 55
0046		S1(I)=S1(I)/U(I+1)		0 56



FORTRAN IV G LEVEL 20		COEFF	DATE = 72286	22/52/18
0047		S2(I)=S2(I)/U(I)	D	57
0048		S3(I)=S3(I)/U(I-1)	O	58
0049	4	CONTINUE	O	59
	C	COEFFICIENTS IN THE FINAL FORM	O	60
0050		DO 5 I=3,NP1	D	61
0051		RL=1./(G2(I)+AU(I)+BU(I)-S2(I))	D	62
0052		AU(I)=(AU(I)+S1(I)-G1(I))*RL	D	63
0053		BU(I)=(BU(I)+S3(I)-G3(I))*RL	D	64
0054	5	CU(I)=CU(I)*RL	D	65
0055		IF (NEQ.EQ.1) GO TO 7	O	66
0056		DO 6 J=1,NPH	O	67
0057		DO 6 I=3,NP1	D	68
0058		RL=1./(G2(I)+A(J,I)+B(J,I)-D(J,I))	D	69
0059		A(J,I)=(A(J,I)-G1(I))*RL	D	70
0060		B(J,I)=(B(J,I)-G3(I))*RL	D	71
0061	6	C(J,I)=C(J,I)*RL	D	72
0062	7	CALL SLIP	O	73
0063		RETURN	O	74
0064		END	O	75-

FORTRAN IV G LEVEL 20		READY	DATE = 72286	22/52/18
0001		SUBROUTINE READY		E 1
0002		COMMON /GEN/ PE1,AMI,AME,OPDX,PREF(2),PR(2),P(2),DEN,AMU,XU,XD,XP, 1XL,DX,INTG,CSALFA,ALPHA,XR,REORS,GAM,ZETA,PPD,TNTD,YSTART,USUP,IDI 2MEN,IHEAT,Z,TU,XSTEP/V/U(200),F(2,200),R(200),RHO(200),OM(200),Y(2 300)/I/N,NP1,NP2,NP3,NEU,NPH,KEX,KIN,KASE,KRAD/B/BETA,GAMA(2),TAU1, 4TAUE,AJ1(2),AJE(2),INDI(2),INDE(2)		E 2 E 3 E 4 E 5 E 6
0003		CALL DENSTY		E 7
0004		CALL RAD (XU,R(1),CSALFA)		E 8
	C	Y NEAR THE I BOUNDARY		E 9
0005		GO TO (1,2,3), KIN		E 10
0006	1	$Y(2) = (1. + BETA) * OM(3) * 4. / ((3. * RHO(2) + RHO(3)) * (U(2) + U(3)))$		E 11
0007		GO TO 4		E 12
0008	2	$Y(2) = 12. * OM(3) / ((3. * RHO(2) + RHO(3)) * (U(2) + U(3) + 4. * U(1)))$		E 13
0009		GO TO 4		E 14
0010	3	$Y(2) = .5 * OM(3) / (RHO(1) * U(1))$		E 15
0011	4	$Y(3) = Y(2) + .25 * OM(3) * (1. / (RHO(3) * U(3)) + 2. / (RHO(3) * U(3) + RHO(2) * U(2)))$		E 16 E 17
	C	Y 'S FOR INTERMEDIATE GRID POINTS		E 18
0012		DO 5 I=4,NP1		E 19
0013	5	$Y(I) = Y(I-1) + .5 * (OM(I) - OM(I-1)) * (1. / (RHO(I) * U(I)) + 1. / (RHO(I-1) * U(I-1)))$		E 20 E 21
	C	Y NEAR THE E BOUNDARY		E 22
0014		$Y(NP2) = Y(NP1) + .25 * (OM(NP2) - OM(NP1)) * (1. / (RHO(NP1) * U(NP1)) + 2. / (RHO(NP1) * U(NP1) + RHO(NP2) * U(NP2)))$		E 23 E 24
0015		GO TO (6,7,8), KEX		E 25
0016	6	$Y(NP3) = Y(NP2) + (1. + BETA) * (OM(NP2) - OM(NP1)) * 4. / ((RHO(NP1) + 3. * RHO(NP2)) * (U(NP1) + U(NP2)))$		E 26 E 27
0017		GO TO 9		E 28
0018	7	$Y(NP3) = Y(NP2) + 12. * (OM(NP2) - OM(NP1)) / ((RHO(NP1) + 3. * RHO(NP2)) * (U(NP2) + U(NP1) + 4. * U(NP3)))$		E 29 E 30
0019		GO TO 9		E 31
0020	8	$Y(NP3) = Y(NP2) + .5 * (OM(NP2) - OM(NP1)) / (RHO(NP3) * U(NP3))$		E 32
0021	9	IF (CSALFA.EQ.0.0) OR (KRAD.EQ.0) GO TO 11		E 33
	C	XXX IS USED TO KILL SHOT IF NECESSARY		E 34
0022		DO 10 I=2,NP3		E 35
0023		XXX=R(1)*R(1)-2.*Y(1)*PE1*CSALFA		E 36
0024		IF (XXX.LT.0.0) XD=2.*XL		E 37
0025		IF (XXX.LT.0.0) GO TO 14		E 38
0026	10	$Y(1) = 2. * Y(1) * PE1 / (R(1) + SQRT(R(1) * R(1) - 2. * Y(1) * PE1 * CSALFA))$		E 39
	C	CHANGED SIGN OF 2 IN THE DENOMINATOR OF ABOVE FOR INTERNAL FLOW		E 40
0027		GO TO 13		E 41
0028	11	DO 12 I=2,NP3		E 42
0029	12	$Y(I) = PE1 * Y(I) / R(1)$		E 43
0030	13	$Y(2) = 2. * Y(2) - Y(3)$		E 44
0031		$Y(NP2) = 2. * Y(NP2) - Y(NP1)$		E 45
	C	CALCULATION OF RADII		E 46
0032		DO 14 I=2,NP3		E 47
0033		IF (KRAD.EQ.0) R(I)=R(1)		E 48
0034		IF (KRAD.NE.0) R(I)=R(1)-Y(I)*CSALFA		E 49
	C	CHANGED SIGN IN EXPRESSION ABOVE FOR INTERNAL FLOW		E 50
0035	14	CONTINUE		E 51
0036		IF (R(NP3).LE.0.0) XD=2.*XL		E 52
0037		IF (Y(NP3).LT.0.0) XD=2.*XL		E 53
0038		RETURN		E 54
0039		END		E 55

FORTRAN	IV	G	LEVEL	20	DENSTY	DATE = 72286	22/52/18	
0001					SUBROUTINE DENSTY		F	1
0002					COMMON /GEN/ PEI,AMI,AME,DPDX,PREF(2),PR(2),P(2),DEN,AMU,XU,XD,XP,		F	2
					IXL,DX,INTG,CSALFA,ALPHA,XR,REGRS,GAM,ZETA,PPD,TWTO,YSTART,USUP,IDI		F	3
					2MFN,1HEAT,Z,TO,XSTEP/V/U(200),F(2,200),R(200),RHO(200),OM(200),Y(2		F	4
					300)/I/N,NP1,NP2,NP3,NEQ,NPH,KEX,KIN,KASE,KRAD		F	5
0003					TNP3=F(1,NP3)-U(NP3)**2/2.		F	6
0004					RHONP3=TNP3**(.1/(GAM-1.))		F	7
0005					DO 1 I=1,NP3		F	8
0006					T=F(1,I)-U(I)**2/2.		F	9
0007	1				RHO(I)=RHONP3*TNP3/T		F	10
0008					RETURN		F	11
0009					END		F	12-

FORTRAN	IV	G	LEVEL	20	ENTRN	DATE = 72286	22/52/18	
0001					SUBROUTINE ENTRN		G	1
0002					COMMON /GEN/ PEI,AMI,AME,DPDX,PREF(2),PR(2),P(2),DEN,AMU,XU,XD,XP,		G	2
					IXL,DX,INTG,CSALFA,ALPHA,XR,REGRS,GAM,ZETA,PPD,TWTO,YSTART,USUP,IDI		G	3
					2MFN,1HEAT,Z,TO,XSTEP/V/U(200),F(2,200),R(200),RHO(200),OM(200),Y(2		G	4
					300)/I/N,NP1,NP2,NP3,NEQ,NPH,KEX,KIN,KASE,KRAD		G	5
0003	1				GO TO (2,3,6), KEX		G	6
0004	2				RETURN		G	7
0005	3				CONTINUE		G	8
	C				THE FOLLOWING AME IS FOR LAMINAR FLOW		G	9
0006					IF (INTG.NE.1) GO TO 5		G	10
0007					DO 4 I=1,NP3		G	11
0008					IF (OM(I).GT.0.9) N9=1		G	12
0009					IF (OM(I).GT.0.9) I=NP3		G	13
0010	4				CONTINUE		G	14
0011					DOM=OM(N9)-OM(N9-1)		G	15
0012					DOM9=OM(N9)-0.9		G	16
0013	5				CONTINUE		G	17
0014					U9=U(N9)-DOM9/DOM*(U(N9)-U(N9-1))		G	18
0015					TERMA=(U(N9)-U(N9-1))/COM		G	19
0016					R9=R(N9)-DOM9/DOM*(R(N9)-R(N9-1))		G	20
0017					RHO9=RHO(N9)-DOM9/DOM*(RHO(N9)-RHO(N9-1))		G	21
0018					VIS9=VISCO(N9)-DOM9/DOM*(VISCO(N9)-VISCO(N9-1))		G	22
0019					CUUP=R(I9)*R(N9)*RHO(N9)*U(N9)*VISCO(N9)		G	23
0020					CUUP=CUUP+R9*R9*RHO9*U9*VIS9		G	24
0021					CUUP=CUUP/(2.*PEI)		G	25
0022					CUU4=R(I9-1)*R(N9-1)*RHO(N9-1)*U(N9-1)*VISCO(N9-1)		G	26
0023					CUU4=CUU4+R9*R9*RHO9*U9*VIS9		G	27
0024					CUU4=CUU4/(2.*PEI)		G	28
0025					G5=2.*CUUP/(DOM*DOM9)		G	29
0026					G6=2.*CUU4/(DOM*(0.9-GM(N9-1)))		G	30
0027					TERMA=G5*(U(N9)-U9)-G6*(U9-U(N9-1))		G	31
0028	3				TERMA=TERMA/TERMB		G	32
0029					U9WIG=USUP*SQRT(2.)*SQRT(1.-PPD**((GAM-1.)/GAM))		G	33
	C				USUP IS READ-IN IN BEGIN IT SUPPRESSES THE B.L.		G	34
0030					TERMC=U9WIG-U9)/DX*DPDX/(RHO9*U9)		G	35
0031					TERMC=TERMC*PEI/TERMB		G	36
0032					AME=TERMA-TERMC		G	37
0033					AMF=AME-0.1*R(1)*AMI		G	38
0034					AME=AME/(0.9*R(NP3))		G	39
0035					RETURN		G	40
0036	6				AME=0.		G	41
0037					RETURN		G	42
0038					END		G	43-

FORTRAN IV G LEVEL 20		FBC	DATE = 72286	22/52/18
0001		SUBROUTINE FBC (X,J,IND,AJFS)	H	1
0002		COMMON /GEN/ PEI,AMI,AME,DPDX,PREF(2),PR(2),P(2),DEN,AMU,XU,XD,XP,	H	2
		1XL,OX,INTG,CSALFA,ALPHA,XR,REORS,GAM,ZETA,PPO,TWTO,YSTART,USUP,IDI	H	3
		2MEN,IHEAT,Z,TD,XSTEP	H	4
	C	TW IS PRESCRIBED IF IHEAT = 1 -- QDOY IS PRESCRIBED IF NOT 1	H	5
0003		IND=1	H	6
0004		AJFS=TWTO	H	7
0005		IF (IHEAT.EQ.1) GO TO 1	H	8
0006		IND=2	H	9
0007		AJFS=0.0	H	10
0008	1	CONTINUE	H	11
0009		RETURN	H	12
0010		END	H	13-

FORTRAN IV G LEVEL 20		MASS	DATE = 72286	22/52/18
0001		SUBROUTINE MASS (XU,XD,AM)	I	1
	C	APPLICABLE TO AN IMPERMEABLE-WALL SITUATION	I	2
0002		AM=0.	I	3
0003		RETURN	I	4
0004		END	I	5-

FURTRAN IV G LEVEL 20		OUTPUT	DATE = 72286	22/52/18
0001		SUBROUTINE OUTPUT	J	1
0002		COMMON /GEN/ PEI,AMI,AME,DPDX,PREF(2),PR(2),P(2),DEN,AMU,XU,XD,XP,	J	2
		1XL,DX,INTG,CSALFA,ALPHA,XK,REORS,GAM,ZETA,PPU,TWTU,YSTART,USUP,IDI	J	3
		2MFN,IHEAT,Z,TU,XSTEP/V/U(200),F(2,200),R(200),RHO(200),DM(200),Y(2	J	4
		300)/C/SC(200),AU(200),BU(200),CU(200),A(2,200),B(2,200),C(2,200)/D	J	5
		4/YP(200),UR(200),RR(200),HR(200),XM(200),PITOT(200),TEMP(200)/E/DS	J	6
		5STAR(300),XRS(300),RHR(300),COSAL(300)/I/N,NP1,NP2,NP3,NEQ,NPH,KEX	J	7
		6,KIN,KASE,KRAD/B/BETA,GAMA(2),TAU1,TAUE,AJI(2),AJE(2),INDI(2),INDE	J	8
		7(2)	J	9
0003		IF (INTG.NE.1) GO TO 1	J	10
0004		AL=ALPHA*180./3.14159265	J	11
0005		WRITE (6,7) (OM(I),I=1,NP3)	J	12
0006		WRITE (6,6) KRAD,IDIMEN,NEQ,KEX,KIN,IHEAT,N	J	13
0007	1	CONTINUE	J	14
0008		DPDXG=DPDX*GAM/(GAM-1.)	J	15
0009		IF (KRAD.EQ.0) DSTAK(INTG)=Y(NP3)-PEI/(R(1)*RHO(NP3)*U(NP3))	J	16
0010		IF (KRAD.EQ.0) GO TO 2	J	17
0011		DSTAR(INTG)=R(1)-SQRT(R(1)**2-2.*CSALFA*(R(1)*Y(NP3)-0.5*CSALFA*Y(	J	18
		INP3)**2-PEI/(RHO(NP3)*U(NP3)))	J	19
0012		IF (CSALFA.NE.0.0) DSTAR(INTG)=DSTAR(INTG)/CSALFA	J	20
0013	2	CONTINUE	J	21
0014		IF (FLOAT(INTG-1)/5..NE.FLOAT((INTG-1)/5)) RETURN	J	22
0015		DO 3 I=1,NP3	J	23
0016		TEMP(I)=F(1,I)-U(I)**2/2.	J	24
0017		XM(I)=U(I)/SQRT((GAM-1.)*TEMP(I))	J	25
0018		XSQ=XM(I)**2	J	26
0019		IF (XM(I).LE.1.0) PITOT(I)=(1.+(GAM-1.)*XSQ/2.)*(GAM/(GAM-1.))	J	27
0020		IF (XM(I).LE.1.0) GO TO 3	J	28
0021		PITOT(I)=(1+(GAM+1.)*XSQ/2.)*(GAM/(GAM-1.))	J	29
0022		PITOT(I)=PITOT(I)*((GAM+1.)/(2.*GAM*XSQ-GAM+1.))*(1./(GAM-1.))	J	30
0023	3	CONTINUE	J	31
0024		SQ2=SQRT(2.)	J	32
0025		DO 4 I=1,NP3	J	33
0026		PITOT(I)=PITOT(I)/PITOT(NP3)	J	34
0027		YR(I)=Y(I)*CSALFA/R(1)	J	35
0028		UR(I)=U(I)/U(NP3)	J	36
0029		RR(I)=RHO(I)/RHO(NP3)	J	37
0030		HR(I)=U(I)/SQ2	J	38
0031	4	CONTINUE	J	39
0032		WRITE (6,8)	J	40
0033		WRITE (6,12) INTG,XU,Z,REORS,GAM,PR(1),ZETA,TWTU,AL,XR,XL	J	41
0034		WRITE (6,13) NP3,DSTAR(INTG),PEI,AME,DPDXG,OX,CSALFA,USUP,PPU,TAU1	J	42
		1,AJI(1)	J	43
0035		WRITE (6,9)	J	44
0036		DO 5 I=1,NP3,2	J	45
0037		WRITE (6,11) (Y(I),F(1,I),UR(I),HR(I),R(I),RHO(I),YR(I),XM(I),TEMP	J	46
		I(1),RR(I),PITOT(I))	J	47
0038	5	CONTINUE	J	48
0039		WRITE (6,10) (Y(NP3),F(1,NP3),UR(NP3),HR(NP3),R(NP3),RHO(NP3),YR(N	J	49
		1P3),XM(NP3),TEMP(NP3),RR(NP3),PITOT(NP3))	J	50
0040		WRITE (6,9)	J	51
0041		RETURN	J	52
	C		J	53
0042	6	FORMAT(////////,20X,'THE INPUT FLAGS ARE',///,25X,'KRAD = ',I1,	J	54
		1//,25X,'IDIMEN = ',I1,///,25X,'NEQ = ',I1,///,25X,'KEX = ',I1,	J	55
		2//,25X,'KIN = ',I1,///,25X,'IHEAT = ',I1,///,25X,'N = ',I3)	J	56

FORTRAN IV G LEVEL 20		OUTPUT	DATE = 72286	22/52/18
0043	7	FORMAT(24H1THE VALUES OF OMEGA ARE/(1P10E11.4))		J 57
0044	8	FORMAT(1H1,4X,'INTG',9X,'XU',11X,'Z',9X,'REURS',7X,'GAMMA',8X,'PR'		J 58
		1,9X,'ZETA',8X,'TW/TO',7X,'ALPHA',8X,'XR',10X,'XL',5X,'NP3',9X,'DS'		J 59
		2TAP',8X,'PEI',9X,'AME',8X,'DP/DX',8X,'DX',8X,'COSALF',7X,'USUP',8X'		J 60
		3,'P/PO',8X,'TAUI',7X,'AJI(1)')/)		J 61
0045	9	FORMAT(6X,'Y',9X,'H/HQ',9X,'U/UE',8X,'U/UM',9X,'R',10X,'RHO',10X,		J 62
		1'Y/R',9X,'M',11X,'T',10X,'N/NE',7X,'PITOT')/)		J 63
0046	10	FORMAT(1P11E12.5,/)		J 64
0047	11	FORMAT(1P11E12.5)		J 65
0048	12	FORMAT(18,4X,1P10E12.4)		J 66
0049	13	FORMAT(18,4X,1P10E12.4,/) )		J 67
0050		END		J 68-

FORTRAN IV G LEVEL 20		PRE	DATE = 72286	22/52/18
0001		SUBROUTINE PRE (X,DPDXX)		K 1
0002		COMMON /GEN/ PEI,AMI,AME,DPDX,PREF(2),PR(2),P(2),DEN,AMU,XU,XD,XP,		K 2
		1XL,DX,INTG,CSALFA,ALPHA,XR,REURS,GAM,ZETA,PPQ,TWTD,YSTART,USUP,10I		K 3
		2MEN,1HEAT,Z,TO,XSTEP/V/U(200),F(2,200),R(200),RHO(200),OM(200),Y(2		K 4
		300)/1/N,NP1,NP2,NP3,NEQ,NPH,KEX,KIN,KASE,KRAD		K 5
0003		DIMENSION XX(300), POP(300)		K 6
0004		IF (INTG.NE.0) GO TO 1		K 7
0005		READ (5,3) LMAX		K 8
0006		READ (5,4) (XX(L),POP(L),L=1,LMAX)		K 9
0007		WRITE (6,5)		K 10
0008		WRITE (6,6) (XX(L),POP(L),L=1,LMAX)		K 11
0009	1	CONTINUE		K 12
0010		L=1		K 13
0011	2	CONTINUE		K 14
0012		L=L+1		K 15
0013		IF (XX(L).LT.X) GO TO 2		K 16
0014		DPDX=(POP(L)-POP(L-1))/(XX(L)-XX(L-1))		K 17
0015		PPQ=POP(L-1)+DPDX*(X-XX(L-1))		K 18
0016		DPDXX=DPDX		K 19
0017		DPDXX=DPDX*(GAM-1.)/GAM		K 20
0018		RETURN		K 21
	C			K 22
0019	3	FORMAT(13)		K 23
0020	4	FORMAT(2E12.0)		K 24
0021	5	FORMAT(1H1,/,8X,'X',12X,'P/PO',/)		K 25
0022	6	FORMAT(1P2E14.5,16)		K 26
0023		END		K 27-

FORTRAN IV G LEVEL 20		RAD	DATE = 72286	22/52/18
0001		SUBROUTINE RAD (X,R1,CALPHA)		L 1
0002		COMMON /GEN/ PEI,AMI,ANE,DPDX,PREF(2),PH(2),P(2),DEN,AMU,XU,XD,XP,		L 2
		1XL,DX,INTG,CSALFA,ALPHA,XR,REORS,GAM,ZETA,PPU,TWTO,YSTART,USUP,IDI		L 3
		2MEN,THEAT,Z,TU,XSTEP/V/U(200),F(2,200),R(200),RHU(200),QM(200),Y(2		L 4
		300)/I/N,NP1,NP2,NP3,NEQ,NPH,KEX,KIN,KASE,KRAD		L 5
	C	APPLICABLE TO NOZZLES WITH CONSTANT LONGITUDINAL RADIUS OF		L 6
	C	CURVATURE OF THE CONVERGING SECTION- CONSTANT WALL HALF ANGLE OF		L 7
	C	DIVERGING SECTION-AND WALL SLOPES MATCHED DOWNSTREAM OF THE THROAT		L 8
0003		IF (INTG.NE.0) GO TO 1		L 9
0004		P12=3.14159265/2.		L 10
0005		ALPHA=ALPHA*P12/90.		L 11
0006		COSALF=COS(ALPHA)		L 12
0007		SINALF=SIN(ALPHA)		L 13
0008		ZWIG=XR*(1.+SINALF)		L 14
0009		XWIG=XR*(P12+ALPHA)		L 15
0010		RWIG=1.+XR*(1.-COSALF)		L 16
0011	1	CONTINUE		L 17
0012		IF (X.GE.XWIG) GO TO 2		L 18
0013		R(1)=1.+XR*(1.-SIN(X/XR))		L 19
0014		CSALFA=SIN(X/XR)		L 20
0015		CALPHA=CSALFA		L 21
0016		M1=R(1)		L 22
0017		ZZ=XR*(1.-COS(X/XR))		L 23
0018		GO TO 3		L 24
0019	2	CONTINUE		L 25
0020		P(1)=(X-XWIG)*SINALF+RWIG		L 26
0021		CSALFA=COSALF		L 27
0022		CALPHA=CSALFA		L 28
0023		P1=R(1)		L 29
0024		ZZ=(X-XWIG)*CSALFA+ZWIG		L 30
0025	3	CONTINUE		L 31
0026		IF (IDIMEN.EQ.0) R1=1.		
0027		ZZ=ZZ-XR		L 32
0028		Z=ZZ		L 33
0029		RETURN		L 34
0030		END		L 35-

FORTRAN IV G LEVEL 20		SLIP	DATE = 72286	22/52/18
0001		SUBROUTINE SLIP		M 1
0002		COMMON /GEN/ PEI, AMI, AME, OPDX, PREF(2), PR(2), P(2), DEN, AMU, XU, XD, XP,		M 2
		1XL, DX, (INTG, CSALFA, ALPHA, XR, REORS, GAM, ZETA, PPO, TWTO, YSTART, USUP, IDI		M 3
		2MEN, IHEAT, Z, TO, XSTEP/1/N, NP1, NP2, NP3, NEQ, NPH, KEX, KIN, KASE, KRAD/V/U		M 4
		3(200), F(2,200), K(200), RHO(200), OM(200), Y(200)/8/BETA, GAMA(2), TAU(		M 5
		4TAUE, AJI(2), AJE(2), (NDI(2), (NDE(2)		M 6
0003		COMMON /L/ AK, ALMG/C/ SC(200), AU(200), BU(200), CU(200), A(2,200), B(2,		M 7
		1200), C(2,200)		M 8
	C	SLIP COEFFICIENTS NEAR THE I BOUNDARY FOR VELOCITY EQUATION		M 9
0004		CU(2)=0.		M 10
0005		CU(NP2)=0.		M 11
0006		GO TO (1,2,3), KIN		M 12
0007	1	BU(2)=0.		M 13
0008		AU(2)=1./(1.+2.*BETA)		M 14
0009		GO TO 5		M 15
0010	2	SQ=84.*U(1)*U(1)-12.*U(1)*U(3)+9.*U(3)*U(3)		M 16
0011		BU(2)=8.*(2.*U(1)+U(3))/(2.*U(1)+7.*U(3)+SQRT(SQ))		M 17
0012		AU(2)=1.-BU(2)		M 18
0013		GO TO 5		M 19
0014	3	BU(2)=0.		M 20
0015		CALL VEFF (2,3,EMU)		M 21
0016		AK1=1./DX-DPDX/(RHO(1)*U(1)*U(1))		M 22
0017		AK2=-U(1)*AK1+DPDX/(RHO(1)*U(1))		M 23
0018		AJ=RHO(1)*U(1)*.25*(Y(2)+Y(3))*2/EMU		M 24
0019		IF (KRAD.EQ.0) GO TO 4		M 25
0020		AU(2)=2./(2.+AJ*AK1)		M 26
0021		CU(2)=-.5*AJ*AK2*AU(2)		M 27
0022		GO TO 5		M 28
0023	4	CU(2)=1./(2.+3.*AJ*AK1)		M 29
0024		AU(2)=CU(2)*(2.-AJ*AK1)		M 30
0025		CU(2)=-CU(2)*4.*AJ*AK2		M 31
	C	SLIP COEFFICIENTS NEAR THE E BOUNDARY FOR VELOCITY EQUATION		M 32
0026	5	GO TO (6,7,8), KEX		M 33
0027	6	AU(NP2)=0.		M 34
0028		BU(NP2)=1./(1.+2.*BETA)		M 35
0029		GO TO 9		M 36
0030	7	SQ=84.*U(NP3)*U(NP3)-12.*U(NP3)*U(NP1)+9.*U(NP1)*U(NP1)		M 37
0031		AU(NP2)=8.*(2.*U(NP3)+U(NP1))/(2.*U(NP3)+7.*U(NP1)+SQRT(SQ))		M 38
0032		BU(NP2)=1.-AU(NP2)		M 39
0033		GO TO 9		M 40
0034	8	AU(NP2)=0.		M 41
0035		CALL VEFF (NP1,NP2,EMU)		M 42
0036		BK1=1./DX-DPDX/(RHO(NP3)*U(NP3)*U(NP3))		M 43
0037		BK2=-U(NP3)*BK1+DPDX/(RHO(NP3)*U(NP3))		M 44
0038		BJ=RHO(NP3)*U(NP3)*.25*(2.*Y(NP3)-Y(NP1)-Y(NP2))*2/EMU		M 45
0039		CU(NP2)=1./(2.+3.*BJ*BK1)		M 46
0040		BU(NP2)=CU(NP2)*(2.-BJ*BK1)		M 47
0041		CU(NP2)=-CU(NP2)*4.*BJ*BK2		M 48
0042	9	IF (NEQ.EQ.1) RETURN		M 49
	C	SLIP COEFFICIENTS NEAR THE I BOUNDARY FOR OTHER EQUATIONS		M 50
0043		DO 20 J=1,NPH		M 51
0044		C(J,2)=0.		M 52
0045		C(J,NP2)=0.		M 53
0046		GO TO (10,12,13), KIN		M 54
0047	10	CALL FBC (XD,J,INDI(J),QI)		M 55
0048		IF (INDI(J,EQ.1) GO TO 11		M 56



FORTRAN IV G LEVEL		20	SLIP	DATE = 72286	22/52/18
0049			AJI(J)=QI		M 57
0050			A(J,2)=1.		M 58
0051			B(J,2)=0.		M 59
0052			C(J,2)=8.*(1.+2.*BETA)*PREF(J)*AJI(J)/(AK*AK*BETA*(1.+BETA)*(1.+BE 1TA)*(3.*RHO(2)+RHO(3))*U(3))		M 60
0053			GO TO 15		M 61
0054	11		F(J,1)=QI		M 62
0055			A(J,2)=(1.+BETA-GAMA(J))/(1.+BETA+GAMA(J))		M 63
0056			B(J,2)=1.-A(J,2)		M 64
0057			GO TO 15		M 65
0058	12		A(J,2)=(U(2)+U(3)-8.*U(1))/(5.*(U(2)+U(3))+8.*U(1))		M 66
0059			GF=(1.-PREF(J))/(1.+PREF(J))		M 67
0060			A(J,2)=(A(J,2)+GF)/(1.+A(J,2)*GF)		M 68
0061			B(J,2)=1.-A(J,2)		M 69
0062			GO TO 15		M 70
0063	13		B(J,2)=0.		M 71
0064			CALL SOURCE (J,I,CS,DS)		M 72
0065			AK1=1./DX-DS		M 73
0066			AK2=-AK1*F(J,1)-CS		M 74
0067			AJF=AJ*PREF(J)		M 75
0068			IF (KRAO.EQ.0) GO TO 14		M 76
0069			A(J,2)=2./(2.+AJF*AK1)		M 77
0070			C(J,2)=-.5*AJF*AK2*A(J,2)		M 78
0071			GO TO 15		M 79
0072	14		C(J,2)=1./(2.+3.*AJF*AK1)		M 80
0073			A(J,2)=C(J,2)*(2.-AJF*AK1)		M 81
0074			C(J,2)=-C(J,2)*4.*AJF*AK2		M 82
	C		SLIP COEFFICIENTS NEAR THE E BOUNDARY FOR OTHER EQUATIONS		M 83
0075	15		GO TO (15,18,19), KEX		M 84
0076	16		CALL FRC (XD,J,INDE(J),QE)		M 85
0077			IF (INDE(J).EQ.1) GO TO 17		M 86
0078	1		AJE(J)=JE		M 87
0079			B(J,NP2)=1.		M 88
0080			A(J,NP2)=0.		M 89
0081			C(J,NP2)=-8.*(1.+2.*BETA)*PREF(J)*AJE(J)/(AK*AK*BETA*(1.+BETA)*(1. 1+BETA)*(RHO(NP1)+3.*RHO(NP2))*U(NP1))		M 90
0082			GO TO 20		M 91
0083	17		F(J,NP3)=QE		M 92
0084			B(J,NP2)=(1.+BETA-GAMA(J))/(1.+BETA+GAMA(J))		M 93
0085			A(J,NP2)=1.-B(J,NP2)		M 94
0086			GO TO 20		M 95
0087	18		B(J,NP2)=(U(NP2)+U(NP1)-8.*U(NP3))/(5.*(U(NP2)+U(NP1))+8.*U(NP3))		M 96
0088			GF=(1.-PREF(J))/(1.+PREF(J))		M 97
0089			B(J,NP2)=(B(J,NP2)+GF)/(1.+B(J,NP2)*GF)		M 98
0090			A(J,NP2)=1.-B(J,NP2)		M 99
0091			GO TO 20		M 100
0092	19		A(J,NP2)=0.		M 101
0093			CALL SOURCE (J,NP3,CS,DS)		M 102
0094			BK1=1./DX-DS		M 103
0095			BK2=-BK1*F(J,NP3)-CS		M 104
0096			BJF=BJ*PREF(J)		M 105
0097			C(J,NP2)=1./(2.+3.*BJF*BK1)		M 106
0098			B(J,NP2)=C(J,NP2)*(2.-BJF*BK1)		M 107
0099			C(J,NP2)=-C(J,NP2)*4.*BJF*BK2		M 108
0100	20		CONTINUE		M 109
0101			RETURN		M 110

FORTRAN IV G LEVEL 20		SLIP	DATE = 72286	22/52/18
0102	END			M 113-

FORTRAN IV G LEVEL 20		SOLVE	DATE = 72286	22/52/18
0001		SUBROUTINE SOLVE (A,B,C,F,NP3)		N 1
	C	THIS SOLVES EQUATIONS OF THE FORM		N 2
	C	$F(I) = A(I)*F(I+1) + B(I)*F(I-1) + C(I)$		N 3
	C	FOR I=2,NP2		N 4
0002		DIMENSION A(NP3), B(NP3), C(NP3), F(NP3)		N 5
0003		NP2=NP3-1		N 6
0004		B(2)=B(2)*F(1)+C(2)		N 7
0005		DO 1 I=3,NP2		N 8
0006		T=1./(1.-B(I)*A(I-1))		N 9
0007		A(I)=A(I)*T		N 10
0008	1	B(I)=(B(I)*B(I-1)+C(I))*T		N 11
0009		DO 2 I=2,NP2		N 12
0010		J=NP2-I+2		N 13
0011	2	F(J)=A(J)*F(J+1)+B(J)		N 14
0012		RETURN		N 15
0013		END		N 16-

FORTRAN IV G LEVEL 20		SOURCE	DATE = 73046	11/33/59
0001		SUBROUTINE SOURCE (J,I,CS,DS)		
0002		COMMON /GEN/ PEI,AMI,AME,OPDX,PREF(2),PK(2),P(2),DEN,AMU,XU,XD,XP,		A 3
		IXL,DX,INTG,CSALFA,ALPHA,XR,REORS,GAM,ZETA,PPD,TWTO,YSTART,USUP,IOI		A 4
		ZMEN,IHEAT,Z,TO,XSTEP/I/N,NP1,NP2,NP3,NEQ,NPH,KEX,KIN,KASE,KRAD/R/R		A 5
		JA(A,GAMA(2),TAUI,TAUE,AJI(2),AJE(2),INDI(2),INDE(2)/V/UI(200),F(2,2		A 6
		400),H(200),RHO(200),OM(200),Y(200)/C/SC(200),AU(200),BU(200),CU(20		A 7
		50),A(2,200),R(2,200),C(2,200)/O/YR(200),UR(200),WR(200),MR(200),XM		A 8
		6(200),PITOT(200),TEMP(200)/E/DSTAR(300),XRS(300),RWRS(300),COSAL(3		A 9
		700)		A 10
0003		CS=SC(I)*(U(I+1)*U(I+1)-U(I)*U(I))/((OM(I+1)-OM(I)))		
0004		CS=CS-SC(I-1)*(U(I)*U(I)-U(I-1)*U(I-1))/((OM(I)-OM(I-1)))		
0005		CS=(1.-L/PREF(J))*CS/((OM(I+1)-OM(I-1)))		
0006		US=0.		
0007		RETURN		
0008		END		

FORTRAN IV G LEVEL 20		VEFF	DATE = 72286	22/52/18
0001		SUBROUTINE VEFF (I,IP1,EMU)		P 1
0002		COMMON /GEN/ PEI,AMI,AME,OPDX,PREF(2),PK(2),P(2),DEN,AMU,XU,XD,XP,		P 2
		IXL,DX,INTG,CSALFA,ALPHA,XR,REORS,GAM,ZETA,PPD,TWTO,YSTART,USUP,IOI		P 3
		ZMEN,IHEAT,Z,TO,XSTEP/V/UI(200),F(2,200),R(200),RHO(200),OM(200),Y(2		P 4
		300)/I/N,NP1,NP2,NP3,NEQ,NPH,KEX,KIN,KASE,KRAD		P 5
0003		T=F(1,1)-U(I)**2/2.		P 6
0004		TT=F(1,IP1)-U(IP1)**2/2.		P 7
0005		T=(T+TT)/2.		P 8
0006		EMU=T**ZETA/(REORS/SQRT(2.))		P 9
0007		RETURN		P 10
0008		END		P 11-

FORTRAN IV G LEVEL	20	VISCO	DATE = 72286	22/52/18	
0001		FUNCTION VISCO (I)			Q 1
0002		CUMMON /GEN/ PE1,AMI,AME,DPDX,PREF(2),PR(2),P(2),DEN,AMU,XU,XD,XP,			Q 2
		1XL,DX,INTG,CSALFA,ALPHA,XR,REGRS,GAM,ZETA,PPU,TWTO,YSTART,USUP,IDI			Q 3
		2MEN,1HEAT,2,TJ,XSTEP/V/U(200),F(2,200),R(200),RHO(200),OM(200),Y(2			Q 4
		300)/I/N,NP1,NP2,NP3,NEQ,NPH,KEX,KIN,KASE,KRAD			Q 5
0003		T=F(1,I)-U(I)**2/2.			Q 6
0004		VISCO=T**ZETA/(REGRS/SQRT(2.))			Q 7
0005		RETURN			Q 8
0006		END			Q 9-

FORTRAN IV G LEVEL	20	WALL	DATE = 72286	22/52/18	
0001		SUBROUTINE WALL			R 1
0002		CUMMON /GEN/ PE1,AMI,AME,DPDX,PREF(2),PR(2),P(2),DEN,AMU,XU,XD,XP,			R 2
		1XL,DX,INTG,CSALFA,ALPHA,XR,REGRS,GAM,ZETA,PPU,TWTO,YSTART,USUP,IDI			R 3
		2MEN,1HEAT,2,TJ,XSTEP/V/U(200),F(2,200),R(200),RHO(200),OM(200),Y(2			R 4
		300)/I/N,NP1,NP2,NP3,NEQ,NPH,KEX,KIN,KASE,KRAD/B/BETA,GAMA(2),TAUI,			R 5
		4TAUE,AJ(12),AJE(2),INDI(12),INDE(2)			R 6
	C	CALCULATION OF BETA FOR THE I BOUNDARY			R 7
0003	1	YI=.5*(Y(2)+Y(3))			R 8
0004		UI=.5*(U(2)+U(3))			R 9
0005		RH=.25*(3.*RHO(2)+RHO(3))			R 10
0006		RE=RH*UI*YI/VISCO(1)			R 11
0007		FP=DPDX*YI/(RH*UI*UI)			R 12
0008		AM=AM1/(RH*UI)			R 13
	C	FOR LAMINAR FLOW AND AM=0 (NEED DIFFERENT EXPRESSION IF F=0)			R 14
0009		S=1./KE-FP/2.			R 15
0010		BETA=RE*(S+FP+AM)			R 16
0011		TAUI=S*RH*UI*UI			R 17
0012		IF (NEQ.EQ.1) RETURN			R 18
	C	CALCULATION OF GAMA 'S FOR THE I BOUNDARY			R 19
0013		DO 2 J=1,NPH			R 20
	C	FOR LAMINAR FLOW AND LIMITING ZERO AM			R 21
0014		SF=1./(PR(J)*RE)			R 22
0015		GAMA(J)=RE*PR(J)*(SF+AM)			R 23
0016		IF (INDI(J).EQ.1) AJI(J)=SF*RH*UI*(2.*F(J,1)-F(J,2)-F(J,3))*5			R 24
0017	2	CONTINUE			R 25
0018		RETURN			R 26
0019		END			R 27-

# APPENDIX IV INITIAL PRESSURE DISTRIBUTION COMPUTER CODE

```

1: C PROGRAM FOR INITIAL PRESSURE DISTRIBUTION
2: C READ (105,14) G,ALPHA,XR,XSTEP,AACT,AEFF,IDIMEN
3: C G=GAMMA (RATIO OF SPECIFIC HEATS)
4: C ALPHA IS DIVERGING NOZZLE WALL HALF ANGLE
5: C XR IS LONGITUDINAL RADIUS OF CURVATURE OF CONVERGING SECTION
6: C XSTEP IS STEP SIZE ALONG X COORDINATE (PERCENT OF LOCAL WALL RAD)
7: C AACT IS THE ACTUAL NOZZLE AREA RATIO
8: C AEFF IS THE EFFECTIVE NOZZLE AREA RATIO
9: C IDIMEN=0 FOR TWO-DIMENSIONAL NOZZLE AND 1 FOR AXISYMMETRIC NOZZLE
10: C XWIG, ZWIG, AND RWIG ARE THE COORDINATES OF THE POINT WHERE THE
11: C NOZZLE WALL SLOPES ARE MATCHED JUST DOWNSTREAM OF THE THROAT
12: C ALPHA=ALPHA*3.14159/180.
13: C NUM=0
14: C PI2=3.14159/2.
15: C COSALF=COSF(ALPHA)
16: C SINALF=SINF(ALPHA)
17: C ZWIG=XR*(1.+SINALF)
18: C XWIG=XR*(PI2+ALPHA)
19: C RWIG=1.+XR*(1.-COSALF)
20: C XTHBAT=XR*PI2
21: C REND=SQRTF(AACT)
22: C IF (IDIMEN.EQ.0) REND=AACT
23: C XEND=XWIG+(REND-RWIG)/SINALF
24: C CONST=(SQRTF(AACT)*SQRTF(AEFF))/(COSALF*(XEND-XWIG)**1.5)
25: C IF (IDIMEN.EQ.0) CONST=(AACT*AEFF)/(COSALF*(XEND-XTHBAT))
26: C ALPHA=ALPHA*180./3.14159
27: C IF (IDIMEN.EQ.0) WRITE(108,18)
28: C IF (IDIMEN.EQ.1) WRITE(108,19)
29: C WRITE (108,15) G,ALPHA,XR,XEND,XSTEP,AACT,AEFF
30: C C1=(G+1.)/2.
31: C C2=(G-1.)/2.
32: C C3=C1/(G-1.)
33: C C4=C1*C3
34: C C5=C4*C2*C3*2.
35: C FM=0.5
36: C X=0.0
37: C R=0.0
38: C DS=0.0
39: 1 CONTINUE
40: C XU=X
41: C X=X+XSTEP*D
42: C IF (X-XWIG) 2,2,4
43: 2 CONTINUE
44: C IF (.NOT. (XU.LT.XTHBAT.AND.X.GT.XTHBAT)) GO TO 3
45: C X=XTHBAT
46: 3 CONTINUE
47: C Z=XR*(1.-COSF(X/XR))
48: C R=1.+XR*(1.-SINF(X/XR))
49: C RINV=R
50: C COSA=SINF(X/XR)
51: C GO TO 5
52: 4 Z=(X-XWIG)*COSALF+ZWIG
53: C R=(X-XWIG)*SINALF+RWIG
54: C COSA=COSALF

```

```

55: DS=CONST*(X-XWIG)**1.5
56: IF (IDIMEN.EQ.0) DS=CONST*(X-XWIG)
57: RINV=R-DS*COSALF
58: 5 A=(1./RINV)**(1+IDIMEN)
59: IF (A-1.0) 7,6,6
60: 6 A=1.0
61: FM1=1.0
62: FM=1.0
63: b=1.0+C2
64: GO TO 12
65: 7 IF (X-PI2*XR) 11,11,9
66: 8 B=(1.+C2*FM1**2)
67: FM=FM1*(A*B**((C3+1.)-C4*FM1**1/(C5*FM1**2-C4**1)
68: IF (ABS*(FM-FM1)-0.00001) 12,11,11
69: 9 CONTINUE
70: IF (FM-1.20) 10,11,11
71: 10 FM=1.20
72: 11 FM1=FM
73: GO TO 8
74: 12 CONTINUE
75: POP=B**((G/(1.-G))
76: NUM=NUM+1
77: Z=Z-XR
78: WRITE (108,16) FM,POP,Z,X,DS,G,RINV,NUM
79: WRITE (106,17) X,POP,NUM
80: IF (X=XEND) 1,1,13
81: 13 CONTINUE
82: STOP
83: C
84: 14 FORMAT(6E10.0,I1)
85: 15 FORMAT(10X,'GAMMA =',F7.3/,10X,
86: 2'ALPHA =',F7.3/,10X,'XR =',F7.3/,10X,'XEND =',F7.3/,10X,'XSTEP
87: 3 =',F7.3/,10X,'AACT =',F7.3/,10X,'AEFF =',F7.3///, 8X,'MI',11X,
88: 4'P/PO',12X,'Z',13X,'X',12X,'DS',12X,'RW',11X,'RINV',7X,'NUM'//)
89: 16 FORMAT(1P7F14.5,I6)
90: 17 FORMAT(2E12.6, 53X, I3)
91: 18 FORMAT(14I,9X, 'ONE-DIMENSIONAL PERFECT GAS EXPANSION FOR A TWO-
92: 1DIMENSIONAL NOZZLE GEOMETRY WITH',10X,'THE ASSUMPTION THAT THE BO
93: 2UNDARY-LAYER DISPLACEMENT THICKNESS VARIES AS (X-XWIG)^(//)
94: 19 FORMAT(14I,9X, 'ONE-DIMENSIONAL PERFECT GAS EXPANSION FOR AN AXISYM
95: 1METRIC NOZZLE GEOMETRY WITH THE',10X,'ASSUMPTION THAT THE BO
96: 2UNDARY-LAYER DISPLACEMENT THICKNESS VARIES AS (X-XWIG)**3/2'//)
97: END

```

UNCLASSIFIED

Security Classification

## DOCUMENT CONTROL DATA - R &amp; D

(Security classification of title, body of abstract and indexing annotation must be entered when the overall report is classified)

1 ORIGINATING ACTIVITY (Corporate author) Arnold Engineering Development Center Arnold Air Force Station, Tennessee 37389		2a. REPORT SECURITY CLASSIFICATION <b>UNCLASSIFIED</b>	
		2b. GROUP N/A	
3 REPORT TITLE <b>VISCOUS EFFECTS IN LOW-DENSITY NOZZLE FLOWS</b>			
4 DESCRIPTIVE NOTES (Type of report and inclusive dates) <b>March 9 to November 30, 1972--Final Report</b>			
5 AUTHOR(S) (First name, middle initial, last name)  <b>David L. Whitfield, ARO, Inc.</b>			
6 REPORT DATE <b>June 1973</b>		7a. TOTAL NO OF PAGES <b>77</b>	7b. NO OF REFS <b>18</b>
8a. CONTRACT OR GRANT NO.  b. PROJECT NO.  c. Program Element 62302F  d.		9a. ORIGINATOR'S REPORT NUMBER(S)  <b>AEDC-TR-73-52</b>  9b. OTHER REPORT NO(S) (Any other numbers that may be assigned this report)  <b>ARO-VKF-TR-73-8</b>	
10 DISTRIBUTION STATEMENT  <b>Approved for public release; distribution unlimited.</b>			
11 SUPPLEMENTARY NOTES  <b>Available in DDC</b>		12. SPONSORING MILITARY ACTIVITY <b>AFRPL/DYSP Edwards Air Force Base California 93523</b>	
13 ABSTRACT <p>Viscous effects in low-density nozzle flows were investigated numerically, and comparisons were made with experimental data. The numerical method of Patankar and Spalding was modified to solve the internal laminar boundary-layer equations for two-dimensional flow or axisymmetric flow with or without transverse curvature. A listing is given of the computer code. Boundary-layer displacement thicknesses for typical nozzle geometries and flow conditions are presented. Solutions were obtained for specific conditions corresponding to experimental data. The result is a relatively fast, simple to use numerical procedure, which is shown to give results in good agreement with experimental data.</p>			

DD FORM 1473  
1 NOV 65

UNCLASSIFIED

Security Classification

UNCLASSIFIED

Security Classification

14.	KEY WORDS	LINK A		LINK B		LINK C	
		ROLE	WT	ROLE	WT	ROLE	WT
	test facilities convergent divergent nozzles rocket nozzle scaling low density wind tunnels numerical analysis						

APBC  
Arnold AFB Tex

UNCLASSIFIED

Security Classification